

TITLE PAGE

Development of a high-resolution emission inventory and its evaluation and application through air quality modeling for Jiangsu Province, China

Yaduan Zhou¹, Yu Zhao^{1,2*}, Pan Mao¹, Qiang Zhang³, Jie Zhang^{2,4}, Liping Qiu¹, Yang Yang¹

1. State Key Laboratory of Pollution Control & Resource Reuse and School of the Environment, Nanjing University, 163 Xianlin Ave., Nanjing, Jiangsu 210023, China

2. Jiangsu Collaborative Innovation Center of Atmospheric Environment and Equipment Technology (CICAEET), Nanjing University of Information Science & Technology, Jiangsu 210044, China

3. Ministry of Education Key Laboratory for Earth System Modeling, Center for Earth System Science, Tsinghua University, Beijing 100084, China

4. Jiangsu Provincial Academy of Environmental Science, 176 North Jiangdong Rd., Nanjing, Jiangsu 210036, China

*Corresponding author: Yu Zhao

Phone: 86-25-89680650; email: yuzhao@nju.edu.cn

ABSTRACT

1
2 Improved emission inventories combining detailed source information are crucial for
3 better understanding the atmospheric chemistry and effectively making emission control
4 policies using air quality simulation, particularly at regional or local scales. With the
5 downscaled inventories directly applied, chemical transport model might not be able to
6 reproduce the authentic evolution of atmospheric pollution processes at small spatial scales.
7 Using the bottom-up approach, a high-resolution emission inventory was developed for
8 Jiangsu China, including SO₂, NO_x, CO, NH₃, volatile organic compounds (VOCs), total
9 suspended particulates (TSP), PM₁₀, PM_{2.5}, black carbon (BC), organic carbon (OC), and CO₂.
10 The key parameters relevant to emission estimation for over 6000 industrial sources were
11 investigated, compiled and revised at plant level based on various data sources and on-site
12 survey. As a result, the emission fractions of point sources were significantly elevated for
13 most species. The improvement of this provincial inventory was evaluated through
14 comparisons with other inventories at larger spatial scales, using satellite observation and air
15 quality modeling. Compared to the downscaled Multi-resolution Emission Inventory for
16 China (MEIC), the spatial distribution of NO_x emissions in our provincial inventory was
17 more consistent with summer tropospheric NO₂ VCDs observed from OMI, particularly for
18 the grids with moderate emission levels, implying the improved emission estimation for small
19 and medium industrial plants by this work. Three inventories (national, regional, and
20 provincial by this work) were applied in the Models-3/Community Multi-scale Air Quality
21 (CMAQ) system for southern Jiangsu October 2012, to evaluate the model performances with
22 different emission inputs. The best agreement between available ground observation and
23 simulation was found when the provincial inventory was applied, indicated by the smallest
24 normalized mean bias (NMB) and normalized mean errors (NME) for all the concerned
25 species SO₂, NO₂, O₃ and PM_{2.5}. The result thus implied the advantage of improved emission
26 inventory at local scale for high resolution air quality modeling. Under the unfavorable
27 meteorology in which horizontal and vertical movement of atmosphere was limited, the
28 simulated SO₂ concentrations at downtown Nanjing (the capital city of Jiangsu) using the
29 regional or national inventories were much higher than observation, implying the

30 overestimated urban emissions when economy or population densities were applied to
31 downscale or allocate the emissions. With more accurate spatial distribution of emissions at
32 city level, the simulated concentrations using the provincial inventory were much closer to
33 observation. Sensitivity analysis of PM_{2.5} and O₃ formation was conducted using the
34 improved provincial inventory through the Brute Force method. Iron & steel and cement
35 plants were identified as important contributors to the PM_{2.5} concentrations in Nanjing. The
36 O₃ formation was VOCs-limited in southern Jiangsu, and the concentrations were negatively
37 correlated with NO_x emissions in urban areas owing to the accumulated NO_x from
38 transportation. More evaluations are further suggested for the impacts of speciation and
39 temporal and vertical distribution of emissions on air quality modeling at regional or local
40 scales in China.

41

42

1 INTRODUCTION

43 With rapid development of economy and growth of energy consumption, eastern China is
44 experiencing severe atmospheric pollution attributed to the large emissions of primary air
45 pollutants and the subsequent formation of secondary pollution, e.g., fine particles and O₃.
46 Relatively high concentrations of surface PM_{2.5} were observed in eastern China based on the
47 national monitoring network (data source: <http://106.37.208.233/>), and only 9.5% out of 190
48 cities with the measurement data reported in 2014 met the National Ambient Air Quality
49 Standard (NAAQS), i.e., 35 µg/m³ for annual PM_{2.5} concentration (MEP, 2012). Under the
50 serious case of air pollution, series of measures have been conducted to reduce the pollutant
51 emissions and to improve the air quality across the country. For example, the National Air
52 Pollution Prevention Action Plan issued in 2013 required strict emission controls on both
53 industry and transportation sectors, and aimed to achieve a 25%, 20% and 15% reduction of
54 annual PM_{2.5} concentration for Beijing-Tianjin-Hebei (JJJ), Yangtze River Delta (YRD), and
55 Pearl River Delta (PRD) region from 2012 to 2017, respectively. Given the non-linear
56 response of ambient concentrations to emissions, chemical transport modeling (CTM) has
57 been widely applied to study the mechanisms of complex pollution processes and the impacts
58 of emission abatement (Zhang et al., 2006; Streets et al., 2007; B. Zhao et al., 2013; Zhang et

59 al., 2012). As the key input of CTM, therefore, improved emission inventories, particularly at
60 regional or local scales, become important for scientific air quality simulation and effective
61 policy making.

62 Progress has been increasingly achieved in emission inventory studies for China.
63 Compared to earlier national emission inventories including those for Transport and Chemical
64 Evolution over the Pacific Mission (TRACE-P, Streets et al., 2003), Intercontinental Chemical
65 Transport Experiment-Phase B (INTEX-B, Zhang et al., 2009), and Regional Emission
66 inventory in Asia (REAS, Ohara et al., 2007; Kurokawa et al., 2013), Tsinghua University
67 developed the Multi-resolution Emission Inventory for China (MEIC,
68 <http://www.meicmodel.org/>), in which the information of large power plants and cement
69 factories was investigated and the uncertainties of emission estimation for those typical
70 sources were reduced (Wang et al., 2014). Besides, high-resolution emission inventories at
71 regional and city scales were gradually established in the developed regions JJJ, YRD and
72 PRD, attributed to better data support and stronger need to combat air pollution (Zheng et al.,
73 2009; S. Wang et al., 2010; Huang et al., 2011; B. Zhao et al., 2012; Zhao et al., 2015).

74 Resulting from various methods and data sources, clear discrepancies exist in different
75 emission inventories in China, both at national (Y. Zhao et al., 2013; Xia et al., 2016) and
76 local scales (Zhao et al., 2015). When applied in CTM, the uncertainties in emission
77 estimation would inevitably lead to bias in air quality simulation, besides the errors of
78 meteorological field modeling and deficiencies of built-in atmospheric chemical mechanisms
79 (Zheng et al., 2012). Based on the Models-3/Community Multi-scale Air Quality (CMAQ)
80 system, for example, Zhang et al. (2014) simulated PM_{2.5} and O₃ concentrations in
81 southeastern United States using the different versions of national emission inventory (NEI),
82 and compared the results with several ground observational datasets. The model performance
83 with updated inventory (NEI05) was much better than that with old one (NEI99), indicating
84 the impacts of emission inventory on the accuracy of CMAQ simulations. Han et al. (2015)
85 conducted NO₂ vertical column simulation for China with CMAQ, and found that the
86 modeled results using INTEX-B inventory were closer to satellite observation than those
87 using REAS. At regional or local scales, emission inventory that incorporates the detailed
88 information of individual sources is assumed to have advantages in air quality research prior

89 to downscaled national inventory that generally applied regional average levels of emission
90 factors due to unavailability of data (Zhao et al., 2015). The benefits of improved emission
91 estimation, spatial and temporal distribution, or chemical speciation of pollutants, however,
92 have not been sufficiently confirmed with CTM. Recently, Yin et al. (2015) conducted CMAQ
93 simulation on O₃ using updated VOC emission inventory for PRD, implying that the reduced
94 uncertainties of total emission estimation and spatial distribution could improve the model
95 performance compared with ground observation.

96 We select Jiangsu, a typical province with well-developed industry in eastern China, to
97 develop and evaluate the high-resolution emission inventory. The geographic location and
98 cities of the province are illustrated in Figure S1 in the supplement. With a total area of 107
99 200 km² and population of 79.2 million in 2012, Jiangsu was the first ranked province in gross
100 domestic product (GDP) per capita in China (NBSC, 2013a; JSNBS, 2013). It accounted for
101 8.0%, 7.6%, 8.9%, and 10.2% of the country's power generation, cement, pig iron, and crude
102 steel production in 2012, respectively (NBSC, 2013b). Intensive energy consumption and
103 industry resulted in heavy air pollution: all the 13 cities had their annual average
104 concentrations of PM_{2.5} exceeding the NAAQS in 2012, with the highest reaching 74 µg/m³ in
105 the capital city, Nanjing. Clear uncertainties exist in current multi-scale emission inventories.
106 Zhao et al. (2015), for example, estimated Nanjing's SO₂ and PM_{2.5} emissions at 165 and 71
107 Gg in 2012, respectively, while the results by Fu et al. (2013) were 131.8 and 35.3 Gg,
108 implying the necessity of improvement and assessment of regional emission inventory, for
109 both scientific and policy implication. In this work, a comprehensive emission inventory for
110 Jiangsu with high temporal and spatial resolutions was first established with the best available
111 data of local emission sources incorporated. This provincial emission inventory was then
112 compared with other inventories and satellite observation to test its improvement on emission
113 estimation and spatial distribution. CMAQ was further applied to indicate the advantage of
114 the provincial inventory prior to downscaled national and regional ones. In particular, the
115 impacts of spatial distribution of emissions on model performance were analyzed for period
116 with unfavorable meteorological condition. Finally, the improved inventory was applied for
117 sensitivity analysis on regional PM_{2.5} and O₃ formation.

118

119

2 DATA AND METHODS

120 **2.1 Methodology of provincial emission inventory development**

121 The emissions of gaseous pollutants (SO₂, NO_x, CO, NH₃ and VOCs), greenhouse gas
122 CO₂, particulate matter (total suspended particulates, TSP, PM₁₀ and PM_{2.5}) and its chemical
123 compositions (black carbon, BC and organic carbon, OC) of anthropogenic origin in Jiangsu
124 were estimated with a bottom-up method. Emission sources were classified into seven main
125 categories, including power plant, industry, solvent use, transportation, residential &
126 commercial, agriculture and other sources. Industry was subdivided into iron & steel, cement,
127 and other industry including nonferrous metal smelting, brick and lime kilns, chemical
128 industry and other industry boilers. Residential & commercial sector included household
129 combustion of fossil fuel and biofuel. Agriculture included livestock and fertilizer usage.
130 Open biomass burning, cooking, and waste (water) disposal, were considered as other sources.
131 The detailed categories were summarized in Table S1 in the supplement. For each category,
132 point, mobile and area sources were defined depending on the detailed levels of information
133 and the emission characteristics. For point sources, information on emission factor and
134 activity level was investigated and compiled for individual plants, and the annual emissions of
135 atmospheric pollutants were calculated using Eq. (1), as described in Zhao et al (2015).

$$136 \quad E_i = \sum_{j,m} AL_{i,j,m} \times EF_{i,j,m} \times (1 - \eta_{i,j,m}) \quad (1)$$

137 where i, j and m represented the pollutant species, individual plant, and fuel/technology type,
138 respectively; AL was the activity level data; EF was the uncontrolled emission factor; and η
139 was removal efficiency of air pollutant control device.

140 Regarded as mobile sources, the emissions of on-road transportation were calculated by
141 the CORPERT model (EEA, 2012) and then spatially allocated based on the road net
142 information of the province. Area sources included non-road transportation, solvent use,
143 residential & commercial sector, agriculture, and small industry plants without detailed
144 information collected. The emissions from non-road transportation and agriculture were
145 estimated following the methods by Zhang et al. (2010) and Dong et al. (2009), respectively.
146 For other sources, the emissions were calculated using Eq. (2)

147

148
$$E_{i,n} = \sum_m AL_{i,m,n} \times EF_{i,m,n} \times (1 - \eta_{i,m,n}) \quad (2)$$

149 where n represented the source type; EF_n and η_n were the average levels of uncontrolled
150 emission factors and removal efficiencies for given source n . For sources without any
151 emission control measure (e.g., residential combustion), $\eta=0$.

152 **2.2 Activity level**

153 The main sources of activity data are summarized by category in Table S1 in the
154 supplement. Most of coals in Jiangsu were used by power and industry sectors, and household
155 accounted for only 0.3% of total coal consumption in the province in 2012 (JSNBS, 2013),
156 indicating the significance to reduce the uncertainties of emission estimation for power and
157 industry plants. Therefore a comprehensive database for power and industrial sector was
158 established with the information collected and modified from the official environmental
159 statistics, Pollution Source Census (PSC, internal data), and on-site survey on large emitters.
160 Parameters including geographical location, combustion/production technology,
161 fuel/burner/boiler type, installed air pollution control device (APCD) and its removal
162 efficiency were investigated for individual plants. Totally 6750 plants were identified as point
163 sources, including 191 power plants, 185 iron & steel plants, 231 cement factories, 707 lime
164 and brick factories, 365 chemical plants and 5071 other industrial factories, as illustrated in
165 Figure S2 in the supplement. In particular, the kilns for combustion and factories for
166 calcination were separately investigated for cement production, and 25% of cement plants
167 contained the both processes. For power, cement, and iron & steel sectors, the aggregated
168 activity levels compiled plant by plant, i.e., the coal consumption of power generation, and
169 the production of cement, clinker, coke, pig iron, and crude steel, were estimated at 108%,
170 95%, 120%, 109%, 104%, and 98% of the provincial statistics, respectively (JSNBS, 2013).
171 The comparison indicates, on one hand, that larger activity levels would be obtained based on
172 detailed investigation of individual emission sources than official statistics for power and
173 most processes of iron & steel sectors. On the other hand, almost complete investigation on
174 point sources was conducted for those sectors, as very small fractions of activities (5% for
175 cement and 2% for steel production) had to be estimated as area sources. For other industrial
176 sectors, smaller fractions of point sources were achieved, e.g., 32% and 36% for ammonia and

177 sulfuric acid production, respectively.

178 For on-road transportation, the input parameters of COPERT 4 include regional
179 meteorological information, vehicle population by type, fleet composition by control stage
180 (China I–IV, equivalent to Euro I–IV), average vehicle speeds, and annual average kilometers
181 traveled (VKT). Monthly mean temperature and relative humidity were obtained from the
182 China Meteorological Data Sharing Service System (<http://www.eservice.gov.cn>).
183 Populations of different vehicle types were derived from statistical yearbooks by city and then
184 converted to the numbers in COPERT 4 categories. The fleet composition by control stage
185 was obtained from the survey by local government (internal data, Zhao et al., 2015). Vehicle
186 speed by road type (i.e., freeway, arterial and residential road) and VKT by vehicle type were
187 determined according to previous studies (Cai and Xie, 2007; Wang et al., 2008) and the
188 guidebook of emission inventory development for Chinese cities (He, 2015). For area sources,
189 the coal consumption of residential activities was directly taken from National Energy
190 Statistic Yearbook (NBSC, 2013c), while that of small industrial plants were calculated by
191 subtracting the coal consumed by industrial point sources from the coal consumption of total
192 industry provided in the provincial energy balance (NBSC, 2013c). The original data on the
193 activity levels of agriculture, solvent use, non-road transportation and open biomass burning
194 were obtained from the provincial or city statistical yearbooks (JSBNS, 2013).

195 **2.3 Emission factor**

196 Following previous studies (Zhao et al., 2008; 2010; 2011; 2012a; 2012b; Y. Zhao et al.,
197 2013), an emission factor database for Jiangsu was established with detailed information and
198 available results of emission measurements on local sources incorporated. For power sector,
199 parameters relevant to emission factors were obtained at individual plant level including
200 installed capacity, fuel type and quality (e.g., sulfur and ash content), combustion technology,
201 and the type and removal efficiencies of APCDs. In particular, the information of APCD
202 installation obtained from provincial environmental statistics and on-site survey was further
203 corrected according to the official documents on APCD projects of power plants published by
204 Ministry of Environment Protection of China
205 (http://www.zhb.gov.cn/gkml/hbb/bgg/201305/t20130506_251654.htm). As summarized in

206 Table S2 in the supplement, the application rates of flue gas desulfurization (FGD), selective
207 catalytic reduction (SCR)/selective non-catalytic reduction (SNCR), and dust collectors for
208 Jiangsu's power plants in 2012 were 97%, 57% and 99% in terms of coal consumption, and
209 the average removal efficiencies of SO₂, NO_x and TSP weighted by coal consumption were
210 calculated at 83.3%, 37.1% and 98.0%, respectively. Combining all the above-mentioned
211 information, the emission factors for individual plant and facility were calculated using the
212 methods developed by Zhao et al. (2010).

213 Table S3 in the supplement summarizes the emission factors of main industrial processes.
214 For iron & steel production, emission factors of the four main manufacturing processes
215 (coking, sintering, pig iron production, and steel making) were estimated combining the
216 unabated emission factors from previous database (Zhao et al., 2011; Y. Zhao et al., 2013) and
217 the investigated information on penetrations and removal efficiencies of APCDs at plant level.
218 Provided in Table S2, 64.3% of Jiangsu's iron & steel plants installed FGD in 2012 and the
219 average SO₂ removal efficiency was estimated at 78.0%. Dust collectors were installed at
220 almost all the furnaces for pig iron production and steel making, with the averages of PM
221 removal efficiency estimated at 96% and 94%, respectively. For cement production, emission
222 factors were calculated for the two main processes, coal combustion and calcination,
223 following Lei et al. (2011). With dust collectors installed at 99% of plants, the average of
224 overall removal efficiency on TSP was estimated at 97.3% according to our plant-by-plant
225 investigation (Table S2).

226 For area sources, emission factors for non-road transportation were obtained from Zhang
227 et al. (2010), Ye et al. (2014) and Fu et al. (2012). Emission factors for household fossil fuel
228 and biofuel combustion were from the summary of field measurements in Y. Zhao et al.
229 (2013). For agricultural activities including livestock and fertilizer use, emission factors were
230 obtained from Dong et al. (2009) and Yin et al. (2010). Emission factors of VOCs were
231 mainly from Wei et al. (2009) with update for typical sources based on limited local
232 measurements and survey (Bo et al., 2008; EEA, 2013; Xia et al., 2014). The source profiles
233 of VOC for Jiangsu were obtained following Li et al. (2014) with the most recent data from
234 domestic results incorporated (Zhao et al., in preparation).

235 **2.4 Temporal and spatial distributions**

236 The monthly variations of emissions from power plants and industrial sources were
237 assumed to be dominated by the variations of electricity generation and typical industrial
238 production, respectively, and those data were obtained from National Bureau of Statistics of
239 China (<http://data.stats.gov.cn/>). As the real-time monitoring on urban traffic was unavailable
240 for the whole province, the temporal distribution of emissions from on-road vehicles in other
241 cities was considered to be the same as Nanjing (Zhao et al., 2015). For other sources, the
242 temporal distributions for Shanghai investigated by Li et al. (2011) were adopted.

243 Different parameters were used to conduct the spatial allocation of emissions by sector.
244 Latitude and longitude of each point source collected from PSC were checked and revised
245 according to Google Earth to avoid the unexpected errors in the existing database (Figure S2
246 in the supplement). The products of GDP (Huang et al., 2014) and population distribution
247 with high resolution at 1km (Fu et al., 2014) were applied to allocate the emissions from
248 industrial area sources and residential & commercial sources, respectively. Emissions from
249 on-road transportation were allocated based on the road net by city. As the ship flow was
250 unavailable, the widths of Yangtze River and the Grand Canal within Jiangsu were used as
251 indicators for ship emissions. Emissions from open biomass burning were allocated by the
252 locations and brightness of agricultural fire spots observed by MODIS (Moderate Resolution
253 Imaging Spectroradiometer, <https://earthdata.nasa.gov/data/near-real-time-data/firms>). NH₃
254 emissions from livestock and fertilizer usage were allocated based on the density of rural
255 population and the distribution of agricultural lands obtained from the land utilization dataset
256 GlobCover 2009 (<http://globalchange.nasdc.cn>).

257 **2.5 Configuration of air quality modeling**

258 The Models-3/Community Multi-scale Air Quality (CMAQ) version 4.7.1 was applied to
259 evaluate the emission inventory for Jiangsu. As shown in Figure 1, three one-way nested
260 domain modeling was conducted, and the spatial resolutions were set at 27, 9 and 3 km
261 respectively in Lambert Conformal Conic projection, centered at (110° E, 34° N) with two
262 true latitudes 25°N and 40°N. The mother domain (D1, 180×130 cells) covered most part of
263 China, Japan and the whole Korea and part of other country. Jiangsu, Zhejiang, Shanghai,

264 Anhui and parts of other provinces were at the second modeling region (D2, 118×97 cells).
265 The third (D3, 124×70 cells) covered the mega city Shanghai and six most developed cities
266 in southern Jiangsu including Nanjing, Changzhou, Zhenjiang, Wuxi, Suzhou and Nantong.
267 The simulation period was selected from October 1 to 31, 2012, with the first five days
268 chosen as spin-up period to provide initial conditions for later simulations.

269 Meteorological fields were provided by the Weather Research and Forecasting Model
270 (WRF) version 3.4 with the main physical options set as Fu et al. (2013), and the outputs were
271 transferred by meteorology chemistry interface professor (MCIP) version 4.2 into the
272 chemistry transport module in CMAQ (CCTM). In WRF, the U.S. Geological Survey (USGS)
273 database was adapted as terrain and land use data, and the first guess field of meteorological
274 modeling was provided by the final analysis dataset (ds083.2) from National Centers for
275 Environmental Prediction (NCEP). Statistical indicators including Bias, Index of Agreement
276 (IOA), and root mean squared error (RMSE) were applied to evaluate the performance of
277 WRF modeling against observation (Baker, 2004; Zhang et al., 2006). Ground observations in
278 three hours interval at meteorological stations were downloaded from National Climatic Data
279 Center (NCDC), including 43 stations in the second modeling domain D2 and 7 stations in the
280 innermost domain D3 (as labeled in Figure 1). The statistics of those indicators for wind
281 speed and direction at 10 m (WS10 and WD10), temperature at 2 m (T2) and relative
282 humidity at 2 m (RH2) for October 2012 in D2 and D3 were summarized in Table S4.
283 Discrepancies between WRF simulations and ground observations were within acceptable
284 range (Emory et al., 2001) and comparable to the results of other studies (Wang et al., 2014).
285 Better agreements were found for simulations of T2 and RH2 than WS10 and WD10. In spite
286 of moderate overestimation by 0.3% and 3.5% in T2 and RH2, the IOA of those two variables
287 were 0.97 and 0.90, indicating the high consistency with observational. Slightly higher than
288 observation in D2 and D3, simulated WS10 might enhance the diffusion process of pollutants
289 in atmosphere eventually and thus lead to underestimation in pollutant concentrations. For
290 WD10, the bias between simulations and observations was 3.6 degree in D3 within the
291 benchmark range (Emory et al., 2001).

292 The carbon bond gas-phase mechanism (CB05) and AERO5 aerosol module were
293 adopted in all the CMAQ modules. The initial concentrations and boundary conditions for

294 first modeling domain was the default clean profile, while for nested domain they were
295 extracted from the CCTM outputs of its mother domain. Anthropogenic emissions used for
296 domains D1 and D2 were obtained from the downscaled MEIC with an original spatial
297 resolution of $0.25^{\circ} \times 0.25^{\circ}$. For Jiangsu domain in D3, three inventories, i.e., downscaled
298 MEIC, the regional inventory of YRD by Fu et al. (2013), and the provincial inventory
299 developed in this work, were used to test the modeling performance and potential
300 improvement in emission estimation. In addition, biogenic emission inventory was from the
301 Model Emissions of Gases and Aerosols from Nature developed under the Monitoring
302 Atmospheric Composition and Climate project (MEGAN-MACC, Sindelarova et al., 2014),
303 and the emission inventories of Cl, HCl and lightning NO_x were from the Global Emissions
304 Initiative (GEIA, Price et al., 1997). The vertical distributions of emissions were directly
305 taken from L. Wang et al. (2010) except for the power sector, as the height of discharge outlet
306 for each plant was available. According to L. Wang et al. (2010), the fractions of emissions of
307 industry sources were 50%, 30% and 20% in layers 1-3, respectively. For the sources near the
308 surface, i.e., transportation, residential & commercial combustion, solvent use, agriculture,
309 and other, emissions were overall allocated to the first vertical layer in the model. The
310 emissions of power plants were concentrated in layers 2-5 with the fractions estimated at 14%,
311 46%, 35% and 5%, respectively, based on the height information of the stacks.

312

313

3 RESULTS

3.1 Emission estimation and sector contribution

314 The total annual emissions of SO_2 , NO_x , CO, TSP, PM_{10} , $\text{PM}_{2.5}$, BC, OC, CO_2 , NH_3 and
315 VOCs were calculated at 1142, 1642, 7680, 2606, 1394, 941, 57, 138, 860458, 1100 and 1747
316 Gg for Jiangsu in 2012, respectively. The emissions by city were provided in Table 1. In
317 general, higher emissions were found in cities in southern Jiangsu with large population and
318 intensive economy and industry than those in northern Jiangsu. Taking 52% of the provincial
319 industrial GDP, Suzhou, Nanjing, and Wuxi were estimated to collectively account for 41%,
320 41%, 35%, 31%, 43% and 39% of the total emissions of SO_2 , NO_x , CO, $\text{PM}_{2.5}$, CO_2 and
321 VOCs, respectively. Xuzhou, different with other cities in northern Jiangsu, had a relative
322

323 high emissions of pollutants due to its well development of large-scale industry. Because of
324 the active agricultural development, NH₃ emissions in Huai'an and Nantong were estimated at
325 195.9 and 187.1 Gg, significantly higher than other cities.

326 Shown in Figure 2 is the detailed sector contribution of pollutants from point, mobile
327 (on-road transportation) and area sources. The point sources including power and industrial
328 plants contributed 84%, 71%, 55%, 83%, 75%, 64%, 41%, 31%, 83%, 2% and 36%, to the
329 total emissions of SO₂, NO_x, CO, TSP, PM₁₀, PM_{2.5}, BC, OC, CO₂, NH₃ and VOCs,
330 respectively. Notably the emission fractions of point sources were larger than those in other
331 regional inventories (Fu, 2009; Tang et al., 2012; B. Zhao et al., 2012), resulting mainly from
332 the compiling and application of information on individual power and industrial plants from
333 varied data sources. Defined as area source, open biomass burning contributed 12%, 19%,
334 23%, 11% and 41% to the total CO, PM₁₀, PM_{2.5}, BC and OC, respectively.

335 The dominant contributors to SO₂ were power plant, iron & steel and other industry, with
336 the emission fractions estimated at 38%, 10% and 45%, respectively. Although the coal
337 consumption in power sector was 3.5 times larger than that in other industry sector (cement
338 and iron & steel production excluded, JSNBS, 2013), smaller contribution to SO₂ emissions
339 were found for coal-fired power plants, implying the benefits of strict control on SO₂
340 emissions from power sector. As shown in Table S2, the application rate and average SO₂
341 removal efficiency of FGD in power sector were significantly higher than those in other
342 industry, suggesting the improvement in SO₂ abatement for industrial coal combustion other
343 than power plants would be an effective measure to further reduce the emissions at present.

344 Power sector was the largest source for NO_x, contributing 41% to the total emissions,
345 while the share of coal consumption of the sector reached 65% (JSNBS, 2013). It thus implied
346 the tightened controls from implementation of new emission standard (GB13223-2011) and
347 improved use of SCR/SNCR on power plants since 2011 compared to other sectors. Compiled
348 from unit level, the average NO_x removal efficiency of SCR/SNCR was calculated at 37% for
349 Jiangsu's power plants in 2012 (Table S2), while Tian et al. (2013) estimated the values for
350 SCR and SNCR at 70% and 25%, respectively, indicating the differences in assessment of
351 emission controls for power sector between the provincial and national emission inventories
352 with varied data sources. Transportation (including on-road and non-road) was estimated to be

353 the second largest sector for NO_x emissions, with the share to the total emissions calculated at
354 24%. Without specific control measures, cement and other industry were estimated to account
355 for 7% and 18% of total NO_x emissions.

356 CO was mainly generated from the manufacturing processes in iron & steel plants. The
357 production of pig iron and crude steel in Jiangsu accounted for 9% and 10% to the national
358 total in 2012, respectively (NBS, 2013), and was higher than other provinces in China except
359 Hebei. Due to the intensive iron & steel industry, the contribution of the sector to the
360 provincial total CO emissions was estimated at 35%. Residential biofuel combustion, open
361 biomass burning and on-road transportation were also large contributors to CO with the
362 emission fractions calculated as 24%, 12% and 11% respectively.

363 For particles, iron & steel and cement production were estimated to be the largest sources,
364 contributing 24% and 27% to the total emissions of PM₁₀, and 27% and 19% to PM_{2.5},
365 respectively. Even with the largest coal consumption among all the sectors, the emissions
366 from power plants were relatively small (6% and 4% to the total PM₁₀ and PM_{2.5} emissions,
367 respectively), resulting mainly from the relatively high penetrations and removal efficiencies
368 of dust collectors. Great differences existed in the sector distribution of BC and OC emissions.
369 Iron & steel was estimated to be the largest source of BC, while open biomass burning and
370 biofuel burning in residential stoves dominated OC, with the shares estimated at 41% and
371 29%, respectively. Moreover, as BC exhausted from the diesel engines was demonstrated to
372 be higher than OC in previous situ measurements (He et al., 2015), BC emissions from
373 non-road transportation (agricultural machines, rural vehicles, ships and construction
374 machines) was estimated more than twice larger than OC.

375 For VOCs, solvent use and other industry including oil refinery, chemical industry and
376 combustion were identified as the largest sources contributing 30% and 29% to total
377 emissions, respectively. In particular, oil refinery and chemical engineering collectively
378 accounted for 74% of the emissions of other industry. Due to lack of investigation on
379 chemical industry plants, the fraction of area sources to the emissions of other industry
380 reached 35%. Transportation and residential cooking are estimated to contribute 12% and 4%
381 to total VOCs emissions, respectively. Livestock and fertilizer use were the two dominating
382 sources of NH₃, with the shares to total emissions estimated at 47% and 45%, respectively.

383 For industry, ammonia production was the main source accounting for half of NH₃ emissions.

384 The spatial distribution of SO₂, NO_x, CO, PM_{2.5}, VOCs and NH₃ emissions were at a
385 resolution of 3×3km were illustrated in Figure S3 in the supplement (Zhou and Zhao, 2016).
386 Outstandingly high emissions of SO₂, NO_x, PM_{2.5} and VOC indicated the existence of large
387 industrial plants, particularly in Suzhou, Nanjing and Wuxi along with the Yangtze River. For
388 CO and NO_x, large emissions were distributed along the road net in the province, reflecting
389 the important contribution of on-road transportation. Unlike other pollutants, high NH₃
390 emissions were more evenly distributed in rural areas as dominated by agricultural activities.

391 **3.2 Comparisons with other studies**

392 Figure 3 compares the emission estimations for Jiangsu between our provincial inventory
393 and previous studies including two regional inventories (Fu et al., 2013; Li et al., 2011) and
394 two national ones (MEIC; Xia et al., 2016). Note this work and Xia et al. (2016) reported the
395 numbers for 2012, while Fu et al. (2013), Li et al. (2011) and MEIC were for 2010. As the
396 emissions from open biomass burning were not included in other inventories except Fu et al.
397 (2013) and this work, two values labeled as A and B were provided for our provincial
398 inventory indicating the emissions with and without biomass open burning, respectively.
399 While provincial economy and energy data were generally applied in all the national/regional
400 inventories, information of individual large emitters were incorporated as well in MEIC, Fu et
401 al. (2013) and Li et al. (2011). For example, the emissions of big plants for power generation,
402 iron & steel and cement production in Jiangsu were partially investigated in Fu et al. (2013)
403 and Li et al. (2011). For MEIC, large fraction of emissions from power generation sector was
404 calculated plant by plant with relatively good data availability, while emissions from other
405 industrial sectors were basically calculated at regional average and spatially allocated as area
406 sources. The results in Fu et al. (2013) were generally smaller than those in other two
407 inventories for 2010.

408 Attributed mainly to the improved use of FGD, the total SO₂ emissions were estimated to
409 decline from 2010 to 2012 for the whole country (Xia et al., 2016) and typical city in Jiangsu
410 (Zhao et al., 2015). It was reasonable to some extent that the SO₂ emissions in Jiangsu
411 estimated in this work for 2012 was less than the 2010 results of Li et al. (2011) and MEIC.

412 Our estimation was 15% lower than the result for Jiangsu extracted from the national
413 inventory by Xia et al. (2016), due mainly to the discrepancies in the penetration and SO₂
414 removal efficiency of FGD applied in the two inventories. Such information was obtained at
415 provincial or national average level by Xia et al. (2016), in contrast to the provincial
416 inventory based on investigation at plant level. For example, Xia et al. (2016) assumed that
417 the penetration rates of wet and dry FGD technologies in coal-fired power sector were 83%
418 and 5% in 2012, with the removal efficiencies estimated at 80% and 40%, respectively, and
419 that there was not any SO₂ control in the remaining 11% of installed capacity at all. According
420 to our plant-based investigation, the controls in Jiangsu were clearly enhanced, as shown in
421 Table S2. As a result, SO₂ emissions from power sector was calculated at 430.0 Gg for
422 Jiangsu 2012 in this work, 42% lower than those in Xia et al. (2016). The result for 2012 in
423 our provincial inventory, however, is very close to the estimation by MEIC for 2010 (437.4
424 Gg), even though the coal consumption of power generation increased 29% for the period
425 2010-2012 (JSNBS, 2013). Besides the uncertainty in emission estimation from varied data
426 sources of the two inventories, the improved use of FGD in the sector could be an important
427 reason for the restrained emissions. Similar fact was found for Nanjing, the capital city of
428 Jiangsu, that the SO₂ emissions of power generation calculated at city level kept stable along
429 with a 25% growth of coal consumption from 2010 to 2012 (Zhao et al., 2015).

430 NO_x emissions in our provincial inventory was slightly higher than those of Li et al.
431 (2011) and clearly lower than the two national inventories. The major difference between the
432 provincial inventory and MEIC was from industry, attributed probably to the application of
433 varied emission factors. With different methods and data sources for certain sectors, the NO_x
434 emissions from industry were calculated at 388.1 and 566.2 Gg respectively by this work and
435 Xia et al. (2016). For on-road transportation, the emission factors were estimated using
436 CORPERT in this work, while they were obtained from limited domestic measurements in
437 Xia et al. (2016). That was also the most important reason for the discrepancies in CO
438 emission estimation between the two studies. For 2010, the NO_x emissions estimated by Fu et
439 al. (2013) was 18% and 36% lower than those by Li et al. (2011) and MEIC, resulting mainly
440 from the higher application rate and removal efficiency of SCR/SNCR technologies for power
441 sector used in Fu et al. (2013).

442 The PM_{2.5} and PM₁₀ emissions in the provincial inventory were estimated to be 6% and
443 23% higher than those of Xia et al. (2016), and the sector contributions were notably different
444 in the two inventories. For example, industry was estimated to contribute 77% and 80% of
445 PM_{2.5} and PM₁₀ in the provincial inventory, much larger than the fractions at 45% and 52% by
446 Xia et al. (2016), respectively. In this work, the PM_{2.5} and PM₁₀ emissions from cement
447 production were calculated at 181 and 384 Gg, i.e., 2.5 and 2.0 times to those in Xia et al.
448 (2016), and the analogue numbers for iron & steel production were 134 and 263 Gg, and 1.8
449 and 1.7 times, respectively. The discrepancies resulted mainly from the inconsistent
450 penetration rates and removal efficiencies of dust collectors determined at national level and
451 from on-site survey at provincial level. Taking cement as an example, all the plants were
452 assumed to be installed with dust collectors, and the national average removal efficiency at
453 99.3% was applied in Xia et al. (2016), clearly larger than that from plant-by-plant survey as
454 shown in Table S2. Note that the particle emissions in the provincial inventory were estimated
455 higher than those in national ones including MEIC and Xia et al. (2016), while the gaseous
456 pollutant emissions were lower except for NH₃ and CO₂. Compared to the emissions for 2010
457 estimated by other studies, the PM_{2.5} and PM₁₀ in our provincial inventory were 58% and 56%
458 larger than Fu et al. (2013) (biomass open burning included), and 24% and 25% larger than Li
459 et al. (2011) (biomass open burning excluded), respectively, beyond the growth rate of 20%
460 for coal consumption during 2010-2012 (NBS, 2011; 2013).

461 The NH₃ emissions of Fu et al. (2013) and Li et al. (2011) were close to each other, while
462 MEIC was only half of them for 2010. Using the results for 2006 from Huang et al. (2012),
463 MEIC made a very low estimation in NH₃ emissions from livestock. The NH₃ emissions for
464 2012 in this work was calculated 11% and 22% larger than the results for 2010 by Fu et al.
465 (2013) and Li et al. (2011), respectively. According to the provincial statistics, the total
466 numbers of livestock and poultry increased 6% and 10% from 2010 to 2012 in Jiangsu
467 (JSNBS, 2013). The growth of activity levels was expected to result in enhanced emissions, as
468 very little progress was achieved for NH₃ control for these years.

469 **3.3 Analysis of spatial distribution of emissions from given sectors**

470 To further explore the discrepancies in emission estimation and spatial distribution from

471 varied data and emission allocation methods, comparisons between MEIC and our provincial
472 inventory were conducted for pollutants from typical sources, including SO₂ from power
473 plants, NO_x from transportation, and PM_{2.5} from industry. The estimates in this work were
474 reallocated into the 0.25°×0.25° grids, consistent with the spatial resolution of MEIC, and the
475 correlation coefficients for emissions in all the grids can be calculated, as shown in Figure 4.
476 Due mainly to the relatively transparent and easily available information of power plants,
477 good consistency was found for SO₂ emissions from power sector in the two inventories, with
478 the correlation coefficient calculated at 0.7 (Figure 4a). Even though the fundamental
479 information of power plants in China is more accessible than other industry sources,
480 mismatches still exist in different data sources. For example, some emission hotspots in our
481 provincial inventory were not totally identical with those in MEIC in Suzhou, Nantong and
482 Nanjing. In contrast to plant-by-plant investigation, the data from existing statistics at national
483 level could not fully track the actual changes in the emitters, e.g., operation of new-built units,
484 shutting down the small ones, or relocation of individual plants. In MEIC, moreover, the SO₂
485 emissions in several grids were estimated extremely small (less than 1 Mg), indicating that
486 part of emissions from power sector was still allocated as area sources based on density of
487 GDP or population. In contrast, all the plants were identified as point sources in the provincial
488 inventory, based on the thorough investigation on individual sources.

489 For NO_x from transportation, the correlation coefficient was calculated at 0.8, indicating
490 an even better consistency than SO₂ from power plants between the two inventories (Figure
491 4b). Although the difference in total emissions was small between our provincial inventory
492 (682 Gg) and MEIC (722 Gg), the estimation of MEIC was notably higher than our result for
493 northern Jiangsu including Yancheng, Huai'an and Suqian, implying the impacts from
494 different ways for emission allocation. In this work, emissions from on-road vehicles were
495 calculated and allocated based on road net that incorporates the information of transportation
496 flow by road grade for each city. For non-road sources, large fraction of emissions was
497 allocated based on the GDP density incorporated with land-use type. In national emission
498 inventories, however, the emissions were first calculated at provincial level, and then
499 downscaled at certain horizontal resolution. Despite of the discrepancies, it could be indicated
500 by the relatively high spatial correlation between the two inventories that using GDP as proxy

501 for emission allocation would be acceptable when detailed information on road net and
502 transportation flow was unavailable, since vehicles were largely concentrated in downtown
503 with the intensive economic activity.

504 For PM_{2.5} from industry, the correlation coefficient was calculated at 0.335, significantly
505 lower than those mentioned above, indicating larger discrepancy in spatial distribution of
506 industrial emissions between provincial and national inventories compared to power and
507 transportation sectors. As shown in Figure 4c, the emission hotspots in the provincial
508 inventory are highly consistent with the locations of large industrial PM_{2.5} emitters (more than
509 10 Gg) estimated in this work, while the emission in MEIC were more distributed in
510 developed cities (e.g., Suzhou) with high density of population or economy. Along with fast
511 urbanization, super industrial sources have gradually been relocated to the rural and suburban
512 areas, and the spatial correlation between industrial emissions and population could thus be
513 weakened. In our provincial inventory, most industrial enterprises were identified as point
514 sources, with the key parameters including geographic location, activity level and removal
515 efficiency of dust collector investigated and corrected at plant level. In MEIC, the emissions
516 were calculated using parameters at regional average level and allocated as area sources
517 according to densities of population and/or economic activity. Without detailed information
518 for individual sources, it might lead to errors in emission estimation and spatial distribution at
519 regional or local scale. According to the survey at plant level, for example, only 20% of the
520 lime factories were installed dust collectors in Jiangsu 2012, much lower than the value
521 (roughly 90%) assumed in national inventories. As a result, the PM_{2.5} emissions from industry
522 were calculated at 570 Gg in our provincial inventory, 78% higher than those of MEIC.

523

524 **4 ASSESSMENT OF THE PROVINCIAL EMISSION INVENTORY**

525 **4.1 Evaluation of spatial distribution of NO_x emissions with satellite observation**

526 Tropospheric NO₂ vertical column density (VCD) retrieved from Ozone Monitoring
527 Instrument (OMI) by the Royal Netherlands Meteorological Institute (Boersma et al., 2011)
528 was employed to test the spatial distribution of NO_x emissions in MEIC and this work.
529 Tropospheric NO₂ over China in this product is consistent with NO₂ data from ground-based

530 measurements with multi-axis DOAS ($R^2=0.96$; Lin et al., 2014). Since clouds reduce the
531 accuracy of satellite measurements, only pixels with cloud fraction ≤ 0.2 have been analyzed.
532 NO_2 VCDs in summer were used due to the short lifetime of NO_2 in atmosphere at high
533 temperature and the difficulty in accumulation for primary emissions with strong air
534 convection. In addition, the summer prevailing wind for Jiangsu was generally from southeast
535 where Shanghai and Zhejiang Province are located (see Figure S1 for the locations of the
536 three regions). Total NO_x emissions of Jiangsu were estimated to be 65% and 282% larger
537 than those of Zhejiang and Shanghai in MEIC, indicating the local sources played an
538 important role in the air pollution formation for the province (Cheng et al., 2011). As Mijling
539 et al. (2013) illustrated satellite observations could be used to evaluate the primary emissions
540 for regions where NO_2 VCDs were mainly affected by local emissions, it was thus feasible to
541 apply the OMI NO_2 VCDs in Jiangsu to assess its NO_x emissions.

542 NO_2 VCDs in July 2010 and 2012 with original spatial resolution of $0.125^\circ \times 0.125^\circ$ were
543 used for comparisons with the emissions in MEIC and our provincial inventory, respectively.
544 To be consistent with MEIC, the emissions in our provincial inventory and the NO_2 VCDs
545 from OMI were first upscaled to $0.25^\circ \times 0.25^\circ$ for the purpose of visualization and correlation
546 analysis. As can be seen in Figure 5a and 5b, clear reduction in summer NO_2 VCDs was
547 found in southern Jiangsu from 2010 to 2012, indicating the benefits of efforts on NO_x
548 abatement since 2011. The NO_2 VCDs in the area along the Yangtze River were notably
549 higher than that in other regions, attributed possibly to the substantial emissions from vessels
550 and small captive power plants of the chemical and refinery industrial parks along the river
551 without stringent controls as big power plants. Shown in Figure 5c and 5d are the spatial
552 distributions of Jiangsu's NO_x emissions in MEIC and our provincial inventory, respectively,
553 and the emission hotspots were generally consistent between the two inventories. Figure 5e
554 and 5f shows the linear regression results between NO_2 VCDs and NO_x emissions in MEIC
555 and the provincial inventory, respectively. The correlation coefficients between VCDs and
556 emissions were separately provided for all the grids and grids in different emission intervals,
557 i.e., top 50%, 50%-75%, and last 25%.

558 The correlation coefficient between NO_2 VCDs and NO_x emissions from the provincial
559 inventory was 0.534, close to that between NO_2 VCDs and MEIC at 0.531. The result

560 indicated that there was no significant difference in spatial distribution of emissions between
561 the national and provincial inventories at the relatively low horizontal resolution. However,
562 great discrepancies existed when the correlation analysis was conducted for grids in different
563 emission intervals. As shown in Figure 5e, the correlation coefficients between VCDs and
564 MEIC emissions were calculated at 0.24 and 0.34, respectively, for the top 50% (20 grids with
565 emissions ranged 32-121 Gg) and last 25% of gridded emissions (161 grids with emissions
566 ranged 0-12 Gg). For our provincial emission inventory, the correlation coefficients were
567 estimated slightly higher at 0.28 and 0.38, respectively, for the top 50% (18 grids with
568 emissions ranged from 30-75 Gg) and last 25% of gridded emissions (176 grids with
569 emissions ranged 0-12 Gg). Moreover, the coefficient between NO₂ VCDs and gridded
570 emissions for the 50% -75% interval in provincial inventory was 0.26, while negative value
571 (-0.07) was calculated for MEIC, indicating that the emission estimation for areas with small
572 and medium sources in the provincial inventory was more consistent with satellite observation.
573 To better quantify the emissions at local scale, the results revealed the practical significance of
574 careful investigation on individual small industrial sources that were usually identified as area
575 sources due to lack of detailed information in national or regional inventories.

576 The comparisons between spatial distribution of VCDs and emissions should be
577 interpreted cautiously, particularly for regions with relatively low values, as the noise to signal
578 ratio in OMI NO₂ increases with decreased VCDs. Moreover, although summer data were
579 applied to mitigate the effects of long lifetime of NO₂ on pollution plums transport and
580 chemical reaction, non-linear relationship still exists between emissions and VCDs. More
581 comparisons between NO₂ from satellite observation and CTM are thus recommended when
582 improved characterization of NO₂ vertical distribution is available for the region.

583 **4.2 Evaluation of multi-scale inventories with CMAQ**

584 As mentioned in Section 2.5, anthropogenic emission inventories at provincial, regional
585 and national scales were applied respectively to explore the impacts of emission input on the
586 performance of city-scale air quality simulation using CMAQ. With the original horizontal
587 resolutions at 0.25×0.25 and 4×4 km, respectively, national (MEIC) and YRD regional
588 inventories (Fu et al., 2013) were reallocated into the D3 of CCTM modeling at 3×3km

589 (Figure 1), consistent with our provincial inventory. The vertical and temporal distributions of
590 the two inventories were assumed to be same as those of our provincial inventory, as indicated
591 in Section 2.4. For the simulation with provincial inventory, emissions inside and outside
592 Jiangsu in D3 were taken from the provincial inventory developed in this study and from the
593 reallocated YRD regional inventory by Fu et al. (2013), respectively. Given the very limited
594 data accessible on air quality for the province in 2012, the available observation data at nine
595 state-operated monitoring sites in Nanjing including six urban sites (Xuanwumen (XWM),
596 Shanxilu (SXL), Zhonghuamen (ZHM), Ruijinlu (RJL), Caochangmen (CCM), and
597 Maigaoqiao (MGQ)), and three suburban sites (Pukou (PKS), Xianlin (XLS) and Olympic
598 sports center (OSC)) were applied to evaluate the simulation performances with different
599 emission inputs (see locations of the nine sites in Figure 1).

600 The hourly ground concentrations from observation and CMAQ simulation for October
601 2012, expressed as the averages for all the monitoring sites in Nanjing, were compared and
602 illustrated in Figure S4 in the supplement for SO₂, NO₂, ozone and PM_{2.5}. Even though all the
603 simulations could well reproduce the time variation of each species, discrepancies existed
604 when different anthropogenic emission inventory were used. The simulated SO₂ and NO₂
605 concentrations using the provincial inventory were notably lower than those with other two
606 inventories. In addition, simulations failed to catch the high PM_{2.5} and O₃ concentrations for
607 some heavy polluted episodes. For example, the average PM_{2.5} ground concentration during
608 October 21st-23rd and 28th-29th were simulated at 40 and 31 μg/m³, 1.4 and 3.2 times lower
609 than observations. Two statistical indicators, normalized mean bias (NMB) and normalized
610 mean error (NME), were applied to evaluate the model performance (Zhang et al., 2006), as
611 summarized in Table 2. Among all the species, the best simulation performance was found for
612 NO₂, with the NMBs ranged within ±30% for different emission. In general, simulations
613 using the provincial emission inventory performed notably better than those with national and
614 regional ones for all the species, and the NMEs and NMBs were calculated at 47%, 33%,
615 44%%, 52% and -10%, -14%, -25%, -43% for SO₂, NO₂, O₃, PM_{2.5} respectively, comparable
616 to previous U.S. studies (Zhang et al., 2006; Wang et al., 2009). The result thus partly
617 confirmed that air quality simulation at local or regional scales would be largely improved

618 when detailed information on individual sources could be incorporated in the emission
619 inventory. Improved model prediction for pollution event was also achieved with provincial
620 inventory. Taking the pollution episode between 8pm on 18th and 5pm on 19th October as an
621 example, the observed PM_{2.5} concentration at CCM site kept increasing from 8pm on 18th with
622 the highest value reaching 114 µg/m³ at 2am on 19th. Simulated PM_{2.5} concentrations with
623 provincial, regional and national inventory at that time were 90, 53 and 45 µg/m³, respectively.
624 The correlation coefficients between observation and simulations with the three inventories
625 were calculated as 0.66, 0.44 and 0.30 during the episode, respectively, indicating the
626 advantage of provincial inventory in the pollution event simulation.

627 Compared to primary pollutants SO₂ and NO₂, species with strong secondary formation
628 process (PM_{2.5} and O₃ in this case) were clearly under predicted by CMAQ, no matter which
629 inventory was applied. Lack of dust emissions in inventories might be one reason for
630 underestimation of PM_{2.5}. Moreover, as the significant composition of PM_{2.5} in eastern China
631 (Yang et al., 2011), secondary organic and inorganic aerosols might be under predicted
632 attribute to the weakness of chemical mechanisms in the version of CMAQ including the
633 transformation of sulfate and the formation of secondary organic aerosols (Wang et al., 2009).
634 For ozone simulation, better performance was found at suburban sites than urban sites, and
635 the lower simulated concentrations than observation could possibly come from the
636 underestimation in precursor VOCs emissions. For example, the NMB was estimated at -26%
637 for PKS, where many chemical industrial plants were located nearby. In addition, the
638 uncertainty of NO_x emission estimation might also contribute to the discrepancy. As indicated
639 by the data from available continuous emission monitoring systems on Jiangsu's power plants,
640 the NO_x emission factors of power sector applied in current inventory might be overestimated
641 for 2012 (unpublished).

642 The total emissions of SO₂ and NO_x in Jiangsu estimated by Fu et al. (2013) was 1126
643 and 1257 Gg, i.e., 9% and 22% lower than the results of our provincial inventory, respectively.
644 Using the regional inventory by Fu et al. (2013), much higher concentrations of SO₂ and NO₂
645 were simulated than observation at the monitoring sites, with the NMBs calculated at 74%
646 and 30%, respectively. Even with larger emissions, in contrast, the NMBs for simulation with

647 our provincial inventory were -10% and -14%, indicating lower simulated concentrations than
648 observation. This result implies the possible impacts of spatial distributions of emissions on
649 air quality modeling. In regional inventory, densities of population and economic activities
650 were generally applied to allocate large fraction of emissions, leading to particularly high
651 emissions in urban areas, as the economy and population was generally centralized in
652 downtown. Given all the monitoring sites in Nanjing are located in urban or suburban areas,
653 air quality simulation using regional emission inventory was thus liable to over predict the
654 ground concentrations at those sites.

655 Spatial distributions of the monthly mean for simulated concentrations using national,
656 regional and provincial inventories were plotted for SO₂, NO₂, PM_{2.5} and O₃ in Figure 6, and
657 the differences between simulations with varied emissions were shown in Figure 7. As the
658 MEIC emissions were greatly averaged when they were directly downscaled from
659 0.25°×0.25° to 3×3 km, the simulated high concentrations using MEIC were broadly
660 distributed in the modeling domain and commonly located in downtown (as indicated in
661 Figure S1), with the large emitters hardly identified (Figure 6a). For results using the regional
662 and provincial inventories, there were several grids with notably outstanding simulated
663 concentrations, indicating the existence of large emitters (Figure 6b and 6c), and differences
664 with the simulation using MEIC were induced (Figure 7a and 7b). As shown in Figure 7c,
665 moreover, clear differences were also detected between simulations using regional and
666 provincial inventories, implying the discrepancy in allocations of high emissions between the
667 two inventories. With the locations of large power, iron & steel, and cement plants
668 incorporated, the YRD regional emission inventory by Fu et al. (2013) allocated a large
669 fraction of emissions from industries as area sources. In contrast, the emissions from most
670 power and industrial plants were calculated based on source-specific information and were
671 precisely allocated in the provincial inventory, avoiding particularly the emission
672 overestimation in downtown. In addition, the simulated NO₂ and O₃ concentrations for
673 regions outside Jiangsu (i.e., Shanghai and part of Zhejiang and Anhui) using the provincial
674 inventory were 22% lower and 40% higher in average than those using the regional one,
675 respectively (Figure 7c), although same emissions (Fu et al., 2013) were used outside Jiangsu
676 for the two inventories. The result indicates that both local and regional emissions were

677 important for the simulations of the secondary pollutant like O₃. Total VOCs emissions for
678 Jiangsu were estimated at 1740 Gg in MEIC, slight higher than those in the regional (1659 Gg)
679 and provincial inventory (1617 Gg), while the simulated monthly mean O₃ concentrations
680 within Jiangsu using MEIC were notably lower than those using the latter two emissions.
681 Categorized by CB05, differences in chemical compositions of VOCs could be found in the
682 three inventories, attributed to the varied source contributions to VOC emissions and to the
683 different source profiles used in emission speciation (Zhao et al., in preparation). For example,
684 the emissions of ethane (ETH) and ethanol (ETHA) with relatively high ozone formation
685 potential in the provincial inventory were 44% and 209% higher than those in MEIC,
686 respectively. Therefore, the total emission amount, spatial distribution of emissions, and the
687 chemical compositions of precursors are all crucial to the accuracy of ozone simulations, and
688 further analysis on those factors are suggested.

689 **4.3 Improved SO₂ simulation under special meteorological condition**

690 To further examine the simulated concentration response to varied emission inputs at
691 local scale, the simulated SO₂ concentrations using national, regional and provincial
692 inventories were compared with observation at three monitoring sites in downtown Nanjing
693 (XWH, RJL and ZHM) for 6th -14th October 2012, as illustrated in Figure 8. The simulated
694 concentrations using our provincial inventory were the most consistent with observation,
695 while apparent overestimation was found for the simulations using national or regional
696 inventories. At 8 pm October 9 (local time), in particular, the SO₂ concentrations were
697 observed at 33, 12, and 14 µg/m³ at XWH, RJL and ZHM sites, respectively, while the
698 simulated concentrations were respectively simulated at 205, 246 and 228 µg/m³ using MEIC,
699 i.e., 5-19 times higher than the observation. The analogue numbers with regional inventory by
700 Fu et al. (2013) even reached 550, 477 and 476µg/m³, i.e., 15-38 times higher than
701 observation. Although concentrations remained over predicted, better performance was
702 achieved when the improved provincial inventory was used, implying its advantage prior to
703 national or regional ones in the high-resolution air quality modeling. The discrepancies in
704 emissions and the simulated meteorological condition including wind velocity and height of
705 planetary boundary layer (PBL) were inspected to understand the very high concentrations

706 from simulation.

707 Figure S5 in the supplement shows the simulated wind fields from 2 pm on 9th to 5am on
708 10th October. From 2 pm on 9th October 9, WS10 in downtown Nanjing started to decline
709 gradually and reached the minimum of 0.22 m/s at 8 pm, simply not beneficial for the
710 horizontal convection of atmosphere. In addition, the monthly average of PBL height at XWH
711 was simulated at 485 m at day and 140 m at night in October. From 5pm on 9th to 10am on
712 10th, however, the average PBL height decreased to 39m, with the minimum simulated at 32
713 m at 11pm on 9th, seriously restricting the vertical diffusion of pollutants. Under the
714 meteorological condition that horizontal and vertical movement of atmosphere were limited,
715 primary pollutants from large emitters would be easily accumulated over time, possibly
716 leading to high concentrations for areas close to the emission sources. In this case, therefore,
717 the simulated SO₂ concentrations would be largely influenced by the emissions from local and
718 nearby sources, as discussed below.

719 The total SO₂ emissions in Nanjing were estimated at 141 Gg in the provincial inventory,
720 2% and 7% higher than those of national and regional ones respectively. Without big
721 difference in total amount, large discrepancies in spatial distribution existed in those
722 inventories, particularly at high horizontal resolution as shown in Figure 9. Downscaled from
723 0.25°×0.25° to 3×3 km, grids with similar emissions were clustered for MEIC and spatial
724 variations in emissions could hardly be detected other than the hotspot in downtown (Figure
725 9c). Notably lower emissions in downtown Nanjing were found in our provincial inventory
726 than the regional one (Figure 9a and 9b). In addition, the grid with maximum SO₂ emissions
727 (15.7 Gg) in the provincial inventory was in the northwestern of Nanjing where a super power
728 plant was located, labeled as the black star (point A) in Figure 9. As a comparison, the grid
729 with the maximum SO₂ emissions in the regional inventory labeled as the black triangle (point
730 B) in Figure 9 was adjacent to the location of A, and its emissions were calculated to be only
731 28% of the result in the provincial one. Given no other super emitters located nearby, we
732 expected that the discrepancy resulted mainly from the varied emission estimation and
733 positioning for the same power plant in the two inventories. According to on-site survey, only
734 one unit out of two for the plant was installed with FGD, and the SO₂ emissions of the plant
735 was estimated at 13.6 Gg, accounting for 87% of the total emissions in the grid. In contrast, a

736 higher FGD installation rate at 85% was uniformly assumed for the power sector in the
737 regional inventory by Fu et al. (2013), leading to possible underestimation in emissions for
738 the plant. The comparison implied that detailed information compiled from individual plants
739 were crucial for estimation and spatial distribution of pollutant emissions at local scales. SO₂
740 emissions at given monitoring sites were extracted from the gridded national, regional and
741 provincial inventories and summarized in Table 3. As most large SO₂ emitters were located in
742 suburban or rural areas, relatively small emissions were found in the provincial inventory for
743 downtown Nanjing where the monitoring sites were located. As large fractions of emissions
744 were allocated by the density of economy and population, however, the SO₂ emissions in the
745 regional emission inventory were estimated at 1791, 1721, 1918, and 1635 Mg at XWH, RJL,
746 ZHM and CCM sites, which were 4-5 times higher than those of our provincial inventory. In
747 MEIC, the emissions at XWH, RJL, ZHM and MGQ sites were identically estimated at 1298
748 Mg from the downscaling approach, and they were also much larger than those in the
749 provincial inventory. Given the unfavorable condition of pollutant transport for 9th-10th
750 October, the overestimation in local emissions around the downtown monitoring sites in the
751 national and regional inventories thus lead to terribly high simulated concentrations, while the
752 results using the provincial one were much more reasonable. The comparison confirms the
753 benefits of precise quantification of emissions on local air quality modeling.

754 Despite of significant improvement, overestimation in SO₂ concentrations still existed in
755 the simulation with our provincial inventory, attributed possibly to the error of meteorology
756 modeling. Here we selected XWH site as an example to conduct the back trajectory analysis
757 using HYSPLIT model (<http://ready.arl.noaa.gov/HYSPLIT.php>). Shown in Figure S6 in the
758 supplement, the air mass reaching the site at 50 m altitude came mainly from northeast at
759 11pm on 9th October. However, it was inconsistent with WRF modeling results, which
760 indicated the dominating wind was from northwest (150°-170°) at that time. As mentioned
761 above, a big power plant was located northwest to XWH (Figure 9a), and the site might partly
762 be influenced by the large emissions from the plant and enhanced concentrations would then
763 be obtained when northwest wind was simulated.

764

5 SENSITIVITY ANALYSIS OF PM_{2.5} AND OZONE FORMATION IN NANJING

Using the improved provincial inventory, the sensitivity of PM_{2.5} and O₃ concentrations to emissions were further analyzed through the Brute-Force method (BFM, Dunker et al., 1996). For PM_{2.5}, four simulation scenarios were designed: Scenario B (the base case) in which the emissions from all types of sources are included; and Scenarios S1, S2, and S3 in which the pollutant emissions of power, iron & steel and cement plants in D3 were zero out, respectively. The changes in simulated PM_{2.5} ground concentrations in S1, S2, and S3 compared to those in base case for October 2012 are illustrated in Figure S7 in the supplement. The average concentration increments in urban area of Nanjing caused by power, iron & steel, and cement plants were calculated respectively at 3, 11 and 7 µg/m³, accounting for 6%, 26% and 16% of the monthly mean PM_{2.5} concentrations, and the maximum increments within the domain reached 10, 72, and 25 µg/m³, respectively. Given the tiny emission fraction of power sector for primary PM_{2.5} (4% in Jiangsu Province) and the small share in the ground layers (15% for 1st plus 2nd vertical layers), its contribution to PM_{2.5} ground concentration was notably lower than those of iron & steel and cement. Summarized in Table 4 are the contributions of power, iron & steel, cement sectors to monthly mean PM_{2.5} at the nine monitoring sites in Nanjing, October 2012. The contributions of the three sectors to average PM_{2.5} concentrations at all the sites were estimated at 8%, 13% and 9%, respectively. Since all the sites are located in the urban or suburban areas, the estimated PM_{2.5} contributions at individual site varied slightly to each other. Besides monthly mean, the hourly maximum and minimum contributions are provided as well in Table 4. The largest hourly contributions from power, iron & steel and cement plants to PM_{2.5} concentrations were 65% at PKS, 89% at MGQ and 58% at both CCM and OCS, respectively. The contributions became negative at 2 pm on 26th October with average PM_{2.5} concentration of all the sites observed as 164 µg/m³ and simulated as 151 µg/m³ under the base case, i.e., increased particle concentrations were simulated at the moment when emissions from given sector was turned off. The result indicated, on one hand, the relatively high uncertainty of simulation for heavy PM pollution episode dominated by regional transport. On the other hand, as the simulated increments were mostly from the elevated sulfate (SO₄²⁻), nitrate (NO₃⁻) and ammonium (NH₄⁺), the negative

794 contributions might also be caused by the complex chemical mechanisms of SO₂ and NO_x
795 reactions with NH₃ under the NH₃-rich condition in YRD (Wang et al., 2011). Intensive
796 real-time observation on chemical composition of PM_{2.5} is thus recommended to better
797 capture and analyze the processes.

798 To explore the sensitivity of O₃ formation to its precursor emissions, two scenarios were
799 set besides the base case: the VOC-abatement scenario with 50% reduction of all
800 anthropogenic VOCs emissions in D3 (Scenario P1), and the NO_x-abatement scenario with
801 50% reduction of NO_x in D3 (Scenario P2). Shown in Figure S8 in the supplement were the
802 average O₃ concentration changes from October 6th to October 15th. The simulated O₃ average
803 concentration from 11am to 5pm declined significantly under Scenario P1, with the maximum
804 reduction at 54 μg/m³ (Figure S8a) within D3, and changes in the downwind region were
805 greater than the upwind. In contrast, the concentrations were generally enhanced under P2
806 with the maximum increment at 19 μg/m³. Similar variation pattern was found for 1-hour
807 maximum O₃ concentration in Figure S8b and monthly mean concentration in Figure S8c.
808 The 1-hour maximum O₃ concentrations in most downwind area of Shanghai and southern
809 Jiangsu decreased 10-20 μg/m³ with the reduction in VOCs emissions, and the concentrations
810 would generally increase 10-30 μg/m³ with the NO_x reduction. The similar patterns of O₃
811 concentration variation in urban and downwind areas in D3 under P1 or P2 scenario indicated
812 that the O₃ formation was VOCs-limited in all those areas in southern Jiangsu. Therefore,
813 VOC emission abatement could be effective for O₃ pollution control in southern Jiangsu,
814 while NO_x abatement might aggravate the pollution in autumn.

815 The temporal changes in the simulated O₃ concentrations between the P1/P2 and base
816 scenarios at urban (XWH, SXL, RJI, MGQ, ZHM and CCM) and suburban sites (XLS, OCS
817 and PKS) in Nanjing were illustrated for October 6th-16th in Figure 10. Simulated O₃
818 concentrations at urban and suburban sites were generally decreased once the VOC emissions
819 declined and the maximum hourly reduction reached 77.3 and 49.6 μg/m³, respectively. In
820 contrast, concentrations were elevated with the NO_x emission reduction and the maximum
821 growth were 78.7 and 15.4 μg/m³, respectively. Under VOCs-limited regime, in general, the
822 O₃ concentration would be little sensitive to the change of NO_x unless it was rich enough to
823 turn to the negative correlation with O₃. Therefore, due to the intensive NO_x emissions from

824 on-road transportation in downtown Nanjing, the variations of O₃ concentrations in P2
825 scenario at urban monitoring sites were notably greater than those at suburban sites. It should
826 be acknowledged that uncertainty existed in the sensitivity analysis, as the brute-force method
827 ignores the nonlinearity of O₃ response to the changes of precursor emissions. With
828 techniques other than brute-force, e.g., ozone source apportionment (OSAT, Li et al., 2012) or
829 tagged species method (Zhang et al., 2011), the nonlinearity mechanism of O₃ formation
830 could be taken into account. Comparisons between results with different methods are further
831 recommended for the region.

832

833

6 CONCLUSIONS

834 The bottom-up approach was applied to develop a high-resolution emission inventory for
835 Jiangsu, with substantial detailed information on local sources incorporated. Key parameters
836 relevant to emission estimation were examined and revised plant by plant including
837 geographic position, energy consumption and removal efficiencies of APCD from various
838 data sources and on-site survey on large emitters. Compared to previous studies, the emission
839 fractions of point sources were significantly enhanced, except for NH₃ and OC, which are
840 mainly from agriculture activities and biomass open burning, respectively. As lower removal
841 efficiencies of dust collectors were obtained from local investigation, larger primary PM
842 emissions were estimated in our provincial inventory than other national or regional ones.
843 Moreover, clear discrepancy existed in spatial distribution of industrial PM_{2.5} emissions
844 between this work and the national inventory MEIC, indicating the uncertainty of emission
845 downscaling from coarse horizontal resolution. The spatial distribution of NO_x emissions in
846 the provincial inventory was more consistent with summer tropospheric NO₂ VCDs observed
847 from OMI than that of MEIC, particularly for the emissions from small and medium industrial
848 plants. WRF-CMAQ air quality modeling system was set up to evaluate the reliability and
849 improvement of the provincial emission inventory by comparing the simulation performance
850 with that using a national (MEIC) and regional one. Among the three inventories, the best
851 agreement was found between the observation and simulation with the provincial one for all
852 the concerned species at the nine monitoring sites in Nanjing, while underestimation existed

853 particularly for PM_{2.5} and O₃ that were strongly influenced by secondary formation. Under the
854 unfavorable meteorology of pollutant transport, extremely high SO₂ concentrations were
855 simulated using the regional and national inventories, while the results using provincial one
856 were much closer to the observation. The results indicated the advantage of improved
857 estimation and spatial distribution of emissions on air quality modeling at regional or local
858 scales. The improved provincial inventory was further applied for the sensitivity analysis on
859 PM_{2.5} and O₃ formation using BFM simulation, and provided the preliminary results for the
860 policy making of regional haze and photochemical pollution control in southern Jiangsu.

861 Limitations remained in the current inventory. Attributed to unavailability of detailed
862 information, the weekly and hourly variation of emissions could not be fully tracked for each
863 city, and the vertical distribution of emissions by sector, depending mainly on the stack height,
864 temperature and flow of flue gas, could not be accurately determined. Instead, empirical data
865 from previous work (Li et al., 2011; L. Wang et al., 2010; 2014) had to be applied, which
866 might be inconsistent with the reality. In addition, some sources were not included in the
867 current inventory, e.g., fugitive dust emissions from construction sites and road transportation,
868 resulting from lack of reliable data and thereby potentially large uncertainties in the emission
869 estimation at provincial level. Finally, the effects of source profiles on air quality modeling,
870 e.g., the speciation of primary PM_{2.5} and VOC, were not fully evaluated. As they are
871 important on the formation of O₃ and secondary particles, more investigations on typical
872 sources and evaluation through chemistry transport modeling are suggested in the future.

873

874

DATA ACCESS

875 The gridded emissions of air pollutants for Jiangsu province 2012 at a horizontal
876 resolution of 3×3 km can be downloaded at
877 <http://www.airqualitynju.com/En/Data/List/Data%20download>.

878

879

ACKNOWLEDGEMENT

880 This work was sponsored by the Natural Science Foundation of China (91644220 and
881 41575142), Natural Science Foundation of Jiangsu (BK20140020), Ministry of Science and
882 Technology of China (2016YFC0201507), Jiangsu Science and Technology Support Program
883 (SBE2014070918), and Special Research Program of Environmental Protection for
884 Commonweal (201509004). We would like to acknowledge Litao Wang from Hebei
885 University of Engineering, Jia Xing from Tsinghua University for the assistance in CMAQ
886 model, and Xiao Fu from Tsinghua University for providing the emission inventory for
887 Yangtze River Delta region, China. Thanks also go to two anonymous reviewers for their very
888 valuable comments to improve this work.

889

890

REFERENCES

- 891 Baker: Meteorological modeling protocol for application to PM_{2.5}/haze/ozone modeling
892 projects, 2004.
- 893 Bo, Y., Cai, H., Xie, S. D.: Spatial and temporal variation of historical anthropogenic
894 NMVOCs emission inventories in China, *Atmos. Chem. Phys.*, 23, 7297-7316, 2008.
- 895 Boersma, K. F., Eskes, H. J., Dirksen, R. J., van der A, R. J., Veefkind, J. P., Stammes, P.,
896 Huijnen, V., Kleipool, Q. L., Sneep, M., Claas, J., Leitão, J., Richter, A., Zhou, Y., and
897 Brunner, D.: An improved tropospheric NO₂ column retrieval algorithm for the Ozone
898 Monitoring Instrument, *Atmos. Meas. Tech.*, 4, 1905–1928, doi:10.5194/amt-4-1905-2011,
899 2011.
- 900 Cai, H., Xie, S. D.: Estimation of vehicular emission inventories in China from 1980 to 2005,
901 *Atmos. Environ.*, 41, 8963-8979, 2007.
- 902 Cheng, Z., Chen, C. H., Huang, C., Huang, H. Y., Li, L., Wang, H. L.: Trans-boundary
903 primary air pollution between cities in the Yangtze River Delta. *Acta Sci. Circum.*, 31,
904 686-694, 2011 (in Chinese).
- 905 Dong, Y. Q., Chen, C. H., Huang, C., Wang, H. L., Li, L., Dai, P., Jia, J. H.: Anthropogenic
906 emissions and distribution of ammonia in Yangtze River Delta, *Acta Sci. Circum.*, 29,
907 1611-1617, 2009 (in Chinese).
- 908 Dunker, A. M., Morris, R. E., Pollack, A. K., Schleyer, C. H., and Yarwood, G.:
909 Photochemical modeling of the impact of fuels and vehicles on urban ozone using auto oil
910 program data, *Environ. Sci. Technol.*, 30, 787–801, 1996.
- 911 EEA (European Environment Agency): COPERT 4-Computer Programme to Calculate
912 Emissions from Road Transport, User Manual (Version 9.0), Copenhagen, Denmark, 2012.

913 EEA (European Environment Agency): EMAP/CORINAIR Emission Inventory
914 Guidebook-2013, <http://www.eea.europa.eu/publications/emep-eea-guidebook-2013>, 2013.

915 Emery, C., Tai, E., Yarwood, G.: Enhanced meteorological modeling and performance
916 evaluation for two Texas episodes, Report to the Texas Natural Resources Conservation
917 Commission, prepared by ENVIRON, International Corp, Novato, CA, 2001.

918 Fu, J. Y., Jiang, D., Huang, Y. H.: 1Km Grid Population Dataset of China
919 (PopulationGrid_China), Global Change Research Data Publishing & Repository,
920 DOI:10.3974/geodb.2014.01.06. V1, 2014.

921 Fu, M. L., Ge, Y. S., Tan, J. W., Zeng, T., Liang, B.: Characteristics of typical non-road
922 machinery emissions in China by using portable emission measurement system, *Sci. Total*
923 *Environ.*, 437, 255-261, 2012.

924 Fu, Q. Y.: Emission inventory and the foundation mechanism of high pollution of fine
925 particulate matters in Shanghai (in Chinese), Ph. D thesis, Fudan University, Shanghai, China,
926 2009.

927 Fu, X., Wang, S. X., Zhao, B., Xing, J., Cheng, Z., Liu, H., and Hao, J. M.: Emission
928 inventory of primary pollutants and chemical speciation in 2010 for the Yangtze River Delta
929 region, China, *Atmos. Environ.*, 70, 39-50, 2013.

930 Han, K. M., Lee, S., Chang, L. S., and Song, C. H.: A comparison study between
931 CMAQ-simulated and OMI-retrieved NO₂ columns over East Asia for evaluation of NO_x
932 emission fluxes of INTEX-B, CAPSS, and REAS inventories, *Atmos. Chem. Phys.*, 15,
933 1913-1938, doi:10.5194/acp-15-1913-2015, 2015.

934 He, K. B.: Multi-resolution Emission Inventory for China (MEIC): model framework and
935 1990–2010 anthropogenic emissions, International Global Atmospheric Chemistry
936 Conference, 17–21 September, Beijing, China, 2012.

937 He, K. B. (eds): Guidebook of Air Pollutant Emission Inventory Development for Chinese
938 Cities, Beijing, 2015 (in Chinese).

939 He, L. Q., Hu, J. N., Zu, L., Song, J. J., Chen, D.: Emission characteristics of exhaust PM_{2.5}
940 and its carbonaceous components from China I to China III heavy-duty diesel vehicles, *Acta*
941 *Scientiae Circumstantiae*, 35, 656-662, 2015 (in Chinese).

942 Huang, C., Chen, C. H., Li, L., Cheng, Z., Wang, H. L., Huang, H. Y., Streets, D. G., Wang,
943 Y. J., Zhang, G. F., and Chen, Y. R.: Emission inventory of anthropogenic air pollutants and
944 VOC species in the Yangtze River Delta region, China, *Atmos. Chem. Phys.*, 11, 4105-4120,
945 2011.

946 Huang, R. J., Zhang, Y., Bozzetti, C., Ho, K. F., Cao, J. J., Han, Y., Daellenbach, K. R.,
947 Slowik, J. G., Platt, S. M., Canonaco, F., Zotter, P., Wolf, R., Pieber, S. M., Bruns, E. A.,
948 Crippa, M., Ciarelli, G., Piazzalunga, A., Schwikowski, M., Abbaszade, G., Schnelle- Kreis,
949 J., Zimmermann, R., An, Z., Szidat, S., Baltensperger, U., Haddad, I. E., and Prevot, A. S.:
950 High secondary aerosol contribution to particulate pollution during haze events in China,
951 *Nature*, 514, 218–222, 2014.

952 Huang, X., Song, Y., Li, M. M., Li, J. F., Huo, Q., Cai, X. H., Zhu, T., Hu, M., and Zhang, H.
953 S.: A high-resolution ammonia emission inventory in China *Global Biogeochem. Cycles*, 26:
954 GB1030, doi:10.1029/2011GB004161, 2012.

955 Huang, Y. H., Jiang, D., Fu, J. Y.: 1Km Grid GDP Data of China (2005, 2010)
956 (GDPGrid_China), Global Change Research Data Publishing & Repository,
957 DOI:10.3974/geodb.2014.01.07. V1, 2014.

958 Huo, H., Wang, M., Zhang, X. L., He, K. B. Gong, H. M., Jiang, K. J., Jin, Y. F., Shi, Y. D., Yu
959 X.: Projection of energy use and greenhouse gas emissions by motor vehicles in China: Policy
960 options and impacts, *Energ. Policy*, 43: 37-48, 2012.

961 JSNBS (Jiangsu Bureau of Statistics): Statistical Yearbook of Jiangsu, Beijing, China
962 Statistics Press, 2011 (in Chinese).

963 JSNBS (Jiangsu Bureau of Statistics): Statistical Yearbook of Jiangsu, Beijing, China
964 Statistics Press, 2013 (in Chinese).

965 Kain, J.: The Kain-Fritsch convective parameterization: An update, *J. Appl. Meteor.*, 43,
966 170-181, 2004.

967 Kurokawa, J., Ohara, T., Morikawa, T., Hanayama, S., Janssens-Maenhout, G., Fukui, T.,
968 Kawashima, K., and Akimoto, H.: Emissions of air pollutants and greenhouse gases over
969 Asian regions during 2000–2008: Regional Emission inventory in Asia (REAS) version 2,
970 *Atmos. Chem. Phys.*, 13, 11019–11058, doi:10.5194/acp-13-11019-2013, 2013.

971 Lei, Y., Zhang, Q., Nielsen, C., He, K. B.: An inventory of primary air pollutants and CO₂
972 emissions from cement production in China, 1990-2020, *Atmos. Environ.*, 45, 147-154, 2011.

973 Li, L., Chen, C. H., Fu, J. S., Huang, C., Streets, D. G., Huang, Y. H., Zhuang, G. F., Wang, J.
974 Y., Jang, C. J., Wang, H. L., Chen, Y. R., and Fu, M. J.: Air quality and emissions in the
975 Yangtze River Delta, China, *Atmos. Chem. Phys.*, 11, 1621-1639,
976 doi:10.5194/acp-11-1621-2011, 2011.

977 Li, M., Zhang, Q., Streets, D. G., He, K. B., Cheng, Y. F., Emmons, L. K., Huo, H., Kang, S.
978 C., Lu, Z., Shao, M., Su, H., Yu, X., and Zhang, Y.: Mapping Asian anthropogenic emissions
979 of non-methane volatile organic compounds to multiple chemical mechanisms, *Atmos. Chem.*
980 *Phys.*, 14, 5617-5638, 2014.

981 Lin, J., Martin, R. V., Boersma, K. F., Sneep, M., Stammes, P., Spurr, R., Wang, P., van
982 Roozendaal, M., Clémer, K., and Irie, H.: Retrieving tropospheric nitrogen dioxide from the
983 Ozone Monitoring Instrument: effects of aerosols, surface reflectance anisotropy, and vertical
984 profile of nitrogen dioxide, *Atmos. Chem. Phys.*, 14, 1441-1461, 2014

985 Ministry of Environmental Protection (MEP): China National Ambient Air Quality Standards,
986 GB3095-2012, MEP, Beijing, China, 2012 (in Chinese).

987 Mijling, B., Vander, A. R. J., Zhang, Q.: Regional nitrogen oxides emission trends in East
988 Asia observed from space, *Atmos. Chem. Phys.*, 13: 12003-12012, 2013.

989 National Bureau of Statistics (NBS): China Statistical Yearbook 2013, China Statistics Press,

990 Beijing, 2013a (in Chinese).

991 National Bureau of Statistics (NBS): China Industry Economy Statistical Yearbook 2012,
992 China Statistics Press, Beijing, 2013b (in Chinese).

993 National Bureau of Statistics (NBS): China Energy Statistical Yearbook 2012, China Statistics
994 Press, Beijing, 2013c (in Chinese).

995 Ohara, T., Akimoto, H., Kurokawa, J., Horii, N., Yamaji, K., Yan, X., and Hayasaka, T.: An
996 Asian emission inventory of anthropogenic emission sources for the period 1980–2020,
997 *Atmos. Chem. Phys.*, 7, 4419–4444, doi:10.5194/acp-7-4419-2007, 2007.

998 Price, C., Penner, J. and Prather, M.: NO_x from lightning, Part I: Global distribution based on
999 lightning physics, *J. Geophys. Res. Atmos.*, 102, D5, DOI: 10.1029/96JD03504, 1997.

1000 Sindelarova, K., Granier, C., Bouarar, I., Guenther, A., Tilmes, S., Stavrou, T., Müller, J.-F.,
1001 Kuhn, U., Stefani, P., and Knorr, W.: Global dataset of biogenic VOC emissions calculated by
1002 the MEGAN model over the last 30 years, *Atmos. Chem. Phys. Discuss.*, 14, 10725-10788,
1003 doi:10.5194/acpd-14-10725-2014, 2014.

1004 Streets, D. G., Bond, T. C., Carmichael, G. R., Fernandes, S. D., Fu, Q., He, D., Klimont, Z.,
1005 Nelson, S. M., Tsai, N. Y., Wang, M. Q., Woo, J.-H., and Yarber, K. F.: An inventory of
1006 gaseous and primary aerosol emissions in Asia in the year 2000, *J. Geophys. Res.*, 108, 8809,
1007 doi:10.1029/2002JD003093, 2003.

1008 Street, D. G., Fu, J. S., Jang, C. J., Hao, J. M., He, K. B., Tang, X. Y., Zhang, Y. H., Wang, Z.
1009 F., Li, Z. P., Zhang, Q., Wang, L. T., Wang, B. Y., Yu, C.: Air quality during the 2008
1010 Beijing Olympic Games, *Atmos. Environ.*, 41, 480-492, 2007.

1011 Tang, X. L., Zhang, Y., Yi, H. H., Ma J. Y., Pu L.: Development a detailed inventory
1012 framework for estimating major pollutants emissions inventory for Yunnan Province, China,
1013 *Atmos. Environ.*, 57, 116-125, 2012.

1014 Tian, H. Z., Liu, K. Y., Hao, J. M., Wang, Y., Gao, J. J., Qiu, P. P., and Zhu, C. Y.: Nitrogen
1015 oxides emissions from thermal power plants in China: Current status and future predictions,
1016 *Environ. Sci. Technol.*, 47, 11350-11357, 2013.

1017 Wang, K., Zhang, Y., Jang, C., Phillip, S., and Wang, B.Y.: Modeling intercontinental air
1018 pollution transport over the trans-Pacific region in 2001 using the Community Multi scale Air
1019 Quality modeling system, *J. Geophys. Res. Atmos.*, 114, D04307,
1020 doi:10.1029/2008JD010807, 2009.

1021 Wang, Q. D., Huo, H., He, K. B., Yao, Z. L., Zhang, Q.: Characterization of vehicle driving
1022 patterns and development of driving cycles in Chinese cities, *Transportation research part D:*
1023 *transport and environment*, 13, 289-297, 2008.

1024 Wang, S. X., Zhao, M., Xing, J., Wu, Y., Zhou, Y., Lei, Y., He, K. B., Fu, L. X., and Hao, J.
1025 M.: Quantifying the air pollutants emission reduction during the 2008 Olympic Games in
1026 Beijing, *Environ. Sci. Technol.*, 44, 2490-2496, 2010.

1027 Wang, S. X., Xing, J., Jang, C. J., Zhu, Y., Fu, J. S., Hao, J. M.: Impact assessment of

1028 ammonia emissions on inorganic aerosols in east China using response surface modeling
1029 technique, *Environ. Sci. Technol.*, 45: 9293-9300, 2011.

1030 Wang, L. T., Jang, C., Zhang, Y., Wang, K., Zhang, Q., Streets, D. G., Fu, C. J., Lei, Y.,
1031 Schreifels, J., He, K. B., Hao, J. M., Lam, Y. F., Lin, J., Meskhidze, N., Voorhees S., Evarts
1032 D., Phillips S.: Assessment of air quality benefits from national air pollution control policies
1033 in China. Part II: Evaluation of air quality predictions and air quality benefits assessment.
1034 *Atmos. Environ.*, 44, 3449-3457, 2010.

1035 Wang, L. T., Wei, Z., Yang, J., Zhang, Y., Zhang, F. F., Su, J., Meng, C. C., and Zhang, Q.:
1036 The 2013 severe haze over southern Hebei, China: model evaluation, source apportionment,
1037 and policy implications, *Atmos. Chem. Phys.*, 14, 3151–3173, doi:10.5194/acp-14-3151-2014,
1038 2014.

1039 Wei, W., Wang, S. X., Chatani, S., Klimont, Z., Cofala, J., and Hao, J. M.: Emission and
1040 speciation of non-methane volatile organic compounds from anthropogenic sources in China,
1041 *Atmos. Environ.*, 42, 4976–4988, 2008.

1042 Xia, S. J., Zhao, Q. Y., Li, B., Shen, G. F.: Anthropogenic source VOCs emission inventory
1043 of Jiangsu Province, *Research of Environmental Sciences*, 27, 120-126, 2014 (in Chinese).

1044 Xia, Y. M., Zhao, Y., Nielsen, C. P.: The benefits of China's efforts in gaseous pollutant
1045 control indicated by the bottom-up emissions and satellite observations, *Atmos. Environ.*, 136,
1046 43-53, 2016.

1047 Xing, J., Zhang, Y., Wang, S. X., Liu, X. H., Cheng, S. H., Zhang, Q., Chen, Y. S., Streets, D.
1048 G., Jang, C. J., Hao, J. M., Wang, W. X.: Modeling study on the air quality impacts from
1049 emission reductions and a typical meteorological conditions during the 2008 Beijing
1050 Olympics, *Atmos. Environ.*, 45, 1786-1798, 2011.

1051 Yang, F., Tan, J., Zhao, Q., Du Z., He, K., Ma, Y., Duan, F., Chen, G., and Zhao, Q.:
1052 Characteristics of PM_{2.5} speciation in representative megacities and across China, *Atmos.*
1053 *Chem. Phys.*, 11, 5207-5219, doi:10.5194/acp-11-5207-2011, 2011.

1054 Ye, S. Q., Zheng, J. Y., Pan, Y. Y., Wang, S. S., Lu, Q., and Zhong, L. J.: Marine emission
1055 inventory and its temporal and spatial characteristics in Guangdong Province, *Acta Sci.*
1056 *Circum.*, 34, 537–547, 2014 (in Chinese).

1057 Yin, S. S., Zheng, J. Y., Zhang, L. J., and Zhong, L. J.: Anthropogenic ammonia emission
1058 inventory and characteristic in the Pearl River Delta region, *Environ. Sci.*, 31, 1146–1151,
1059 2010 (in Chinese).

1060 Yin, S. S., Zheng, J. Y., Lu, Q., Yuan, Z. B., Huang, Z. J., Zhong, L. J., Lin, H.: A refined
1061 2010-based VOC emission inventory and its improvement on modeling regional ozone in the
1062 Pearl River Delta Region, China, *Sci. Total Environ.*, 514, 426-438, 2015.

1063 Zhang, H. L., Li, J. Y., Ying, Q., Yu, J. Z., Wu, D., Cheng, Y., He, K. B., Jiang, J. K.: Source
1064 apportionment of PM_{2.5} nitrate and sulfate in China using a source-oriented chemical transport
1065 model, *Atmos. Environ.*, 62, 228-242, 2012.

1066 Zhang, L. J., Zheng, J. Y., Yin, S. S., Peng, K., and Zhong, L. J.: Development of non-road
1067 mobile source emission inventory for the Pearl River Delta region, *Environ. Sci.*, 31, 886-891,
1068 2010 (in Chinese).

1069 Zhang, Q., Streets, D. G., Carmichael, G. R., He, K., Huo, H., Kannari, A., Klimont, Z., Park,
1070 I., Reddy, S., Fu, J. S., Chen, D., Duan, L., Lei, Y., Wang, L., and Yao, Z.: Asian emissions in
1071 2006 for the NASA INTEX-B mission, *Atmos. Chem. Phys.*, 9, 5131-5153,
1072 doi:10.5194/acp-9-5131-2009, 2009.

1073 Zhang, Y. and Carmichael, G. R.: The role of mineral aerosol in tropospheric chemistry in
1074 East Asia—a model study, *J. Appl. Meteorol.*, 38, 353-366, 1999.

1075 Zhang, Y., Liu, P., Pun, B., Seigneur, C.: A comprehensive performance evaluation of
1076 MM5-CMAQ for the Summer 1999 Southern Oxidants Study episode—Part I: Evaluation
1077 protocols, databases, and meteorological predictions, *Atmos. Environ.*, 40, 4825-4838, 2006.

1078 Zhang, Y., Wang, W., Wu, S.-Y., Wang, K., Minoura, H., Wang, Z. F.: Impacts of updated
1079 emission inventories on source apportionment of fine particle and ozone over the southeastern
1080 U.S., *Atmos. Environ.*, 88, 133-154, 2014.

1081 Zhao, B., Wang, P., Ma, J. Z., Zhu, S., Pozzer, A., and Li, W.: A high-resolution emission
1082 inventory of primary pollutants for the Huabei region, China, *Atmos. Chem. Phys.*, 12,
1083 481-501, doi:10.5194/acp-12-481-2012, 2012.

1084 Zhao, B., Wang, S. X., Dong, X. Y., Wang, J. D., Duan, L., Fu, X., Hao, J. M., and Fu, J. S.:
1085 Environmental effects of the recent emission changes in China: implications for particulate
1086 matter pollution and soil acidification, *Environ. Res. Lett.*, 8, 24-31, 2013.

1087 Zhao, Y., Wang, S.X., Duan, L., Lei, Y., Cao, P.F., and Hao, J.M.: Primary air pollutant
1088 emissions of coal-fired power plants in China: current status and future prediction. *Atmos.*
1089 *Environ.*, 42, 8442-8452, 2008.

1090 Zhao, Y., Wang, S. X., Nielsen, C. P., Li, X. H., and Hao, J. M.: Establishment of a database
1091 of emission factors for atmospheric pollutants from Chinese coal-fired power plants, *Atmos.*
1092 *Environ.*, 44, 1515-1523, 2010.

1093 Zhao, Y., Nielsen, C. P., McElroy, M. B., Zhang, L., and Zhang, J.: CO emissions in China:
1094 uncertainties and implications of improved energy efficiency and emission control, *Atmos.*
1095 *Environ.*, 49, 103-113, 2012a.

1096 Zhao, Y., Nielsen, C. P., and McElroy, M. B.: China's CO₂ emissions estimated from the
1097 bottom up: Recent trends, spatial distributions, and quantification of uncertainties, *Atmos.*
1098 *Environ.*, 59, 214-223, 2012b.

1099 Zhao, Y., Zhang, J., Nielsen, C. P.: The effects of recent control policies on trends in
1100 emissions of anthropogenic atmospheric pollutants and CO₂ in China, *Atmos. Chem. Phys.*,
1101 13, 487-508, 2013.

1102 Zhao, Y., Qiu, L. P., Xu, R. Y., Xie, F. J., Zhang, Q., Yu, Y. Y., Nielsen, C. P., Qin, H. X.,
1103 Wang, H. K., Wu, X. C., Li, W. Q., and Zhang, J.: Advantages of a city-scale emission

- 1104 inventory for urban air quality research and policy: the case of Nanjing, a typical industrial
1105 city in the Yangtze River Delta, China, *Atmos. Chem. Phys.*, 15, 12623-12644,
1106 doi:10.5194/acp-15-12623-2015, 2015.
- 1107 Zhao, Y., Mao, P., Zhou, Y., Yang, Y., Zhang, J., Wang, S., Dong, Y., Xie, F., Yu, Y., and Li,
1108 W.: Improved provincial emission inventory and speciation profiles of anthropogenic
1109 non-methane volatile organic compounds: a case study for Jiangsu, China, in preparation.
- 1110 Zheng, J. Y., Zhang, L. J., Che, W. W., Zheng, Z., and Yin, S. S.: A highly resolved temporal
1111 and spatial air pollutant emission inventory for the Pearl River Delta region, China and its
1112 uncertainty assessment, *Atmos. Environ.*, 43, 5112–5122, 2009.
- 1113 Zheng, J. Y., Fu, F., Li, Z. C., Wang, S. S., Zhong, L. J.: Implementation and evaluation of
1114 uncertainty propagation using stochastic response surface method based on the CMAQ model,
1115 *Acta Sci. Circum.*, 32, 1289-1298, 2012 (in Chinese).
- 1116 Zhou, Y and Zhao, Y.: Emissions Jiangsu China 2012, available at
1117 <http://www.airqualitynju.com/En/Data/List/Data%20download>, 2016

FIGURE CAPTIONS

1118

1119 **Figure 1. Modeling domain and locations of 43 meteorological and 9 air quality**
1120 **monitoring sites.**

1121 **Figure 2. Source contributions to total estimated emissions by species in Jiangsu 2012.**
1122 **Colors indicate the sectors and the shade patterns indicate the source type (point, mobile**
1123 **and area).**

1124 **Figure 3. Comparison between the emissions estimated in this work and other studies**
1125 **for Jiangsu. A and B indicate the emissions without and with open biomass burning,**
1126 **respectively.**

1127 **Figure 4. Spatial distributions (a-c) and linear regression (d) of certain pollutant**
1128 **emissions from typical sources estimated in our provincial inventory and MEIC. (a) SO₂**
1129 **from power plant; (b) NO_x from transportation; (c) PM_{2.5} from industry. The black**
1130 **points indicate the locations of plants with PM_{2.5} emissions larger than 10 Gg estimated**
1131 **in this work.**

1132 **Figure 5. Spatial distributions of NO₂ VCDs observed by OMI in Jiangsu in 2010 (a) and**
1133 **2012 (b), and those of Jiangsu's NO_x emissions from MEIC (c) and our provincial**
1134 **inventory (d) at the resolution of 0.25°×0.25°. Linear regressions of gridded VCDs and**
1135 **emissions are illustrated for MEIC (e) and our provincial inventory (f).**

1136 **Figure 6. Spatial distributions of the monthly means of simulated SO₂, NO₂, PM_{2.5} and**
1137 **O₃ concentrations using the national, regional and provincial emission inventories for**
1138 **October 2012.**

1139 **Figure 7. The differences in the monthly means of simulated SO₂, NO₂, PM_{2.5} and O₃**
1140 **concentrations using different emission inventories: (a) Provincial–national; (b)**
1141 **Regional–national; and (c) provincial–regional. The black star A and triangle B referred**
1142 **to the locations of grids with maximum SO₂ emissions in provincial and regional**
1143 **inventory.**

1144 **Figure 8. The observed and simulated hourly SO₂ concentrations (expressed with 3-h**
1145 **interval) using the national, regional, and provincial inventories at XWH (a), RJL (b),**
1146 **and ZHM (c) from October 6th to 13th, 2012.**

1147 **Figure 9. Spatial distributions of the estimated SO₂ emissions in Nanjing at the**
1148 **resolution of 3×3km in the provincial (a), regional (b) and national emission inventory**
1149 **(c). The black dots indicate the locations of given air quality monitoring sites. The black**
1150 **star (point A) indicates the location of the power plant with the largest SO₂ emissions**
1151 **estimated in the provincial inventory. The black triangle (point B) indicates the**
1152 **speculated position of the same power plant in the regional inventory.**

1153 **Figure 10. The changes in simulated O₃ concentrations at urban (XWH, SXL, RJL,**
1154 **MGQ, ZHM, and CCM) and suburban air quality monitoring sites (XLS, OSC, and**
1155 **PKS) in Nanjing under P1 (a) and P2 (b) scenarios compared to the base case for 6th-16th**
1156 **October 2012.**

TABLES

Table 1. The estimated annual emissions by city for Jiangsu 2012 (unit: million metric tons (Tg) for CO₂ and kilo metric tons (Gg) for other species).

City	SO ₂	NO _x	CO	TSP	PM ₁₀	PM _{2.5}	BC	OC	CO ₂	NH ₃	VOCs
Southern											
Nanjing	140.6	210.5	742.9	157.3	97.3	75.8	5.8	7.1	97.1	64.2	221.9
Suzhou	220.8	286.7	1383.3	380.6	194.9	137.3	9.8	11.0	184.4	144.8	297.8
Wuxi	107.7	180.0	545.5	271.3	126.9	77.2	3.4	9.6	84.5	24.2	167.2
Changzhou	104.0	107.7	734.6	413.3	194.6	126.2	3.6	7.5	65.2	33.4	104.2
Zhenjiang	44.0	89.6	231.6	143.3	66.8	40.9	1.9	6.6	53.0	38.1	55.4
Central											
Nantong	76.8	130.1	443.4	244.9	108.2	66.0	4.8	9.3	51.6	181.7	162.2
Yangzhou	55.3	93.9	310.7	54.1	39.9	31.1	2.6	8.5	52.1	83.1	82.5
Taizhou	56.6	70.5	315.1	207.6	98.2	52.3	2.7	8.8	31.4	100.7	76.9
Northen											
Xuzhou	138.9	232.5	805.5	223.2	146.5	101.9	6.1	19.1	139.2	49.2	161.2
Huai'an	52.2	61.5	590.0	97.4	64.5	49.5	3.7	12.0	32.5	195.9	78.6
Yancheng	49.9	78.5	639.7	203.8	111.8	72.0	5.6	16.1	28.2	101.0	185.0
Lianyungang	60.6	61.0	571.1	131.0	89.0	68.6	3.9	11.9	28.3	25.1	78.0
Suqian	34.1	39.7	366.8	77.8	55.5	42.3	3.2	11.0	12.9	59.1	76.4
Total	1141.5	1642.2	7680.0	2605.6	1394.0	941.1	57.0	138.5	860.5	1100.3	1747.3

Table 2. Model performance statistics for concentrations of given species from observation and CMAQ simulation using the national, regional and provincial inventories at the nine air quality monitoring sites in Nanjing for October 2012.

Pollutants	National (MEIC)		Regional (Fu et al., 2013)		Provincial (this work)	
	NMB	NME	NMB	NME	NMB	NME
SO ₂	48.45%	76.53%	74.08%	95.04%	-9.97%	47.49%
NO ₂	21.02%	35.99%	29.84%	43.45%	-14.47%	33.22%
O ₃	-65.55%	68.57%	-53.93%	61.59%	-24.98%	44.29%
PM _{2.5}	-51.63%	55.32%	-49.16%	56.00%	-43.64%	51.81%

Note: NMB and NME were calculated using following equations (P and O indicate the results from modeling prediction and observation, respectively):

$$NMB = \frac{\sum_{i=1}^n (P_i - O_i)}{\sum_{i=1}^n O_i} \times 100\%; \quad NME = \frac{\sum_{i=1}^n |P_i - O_i|}{\sum_{i=1}^n O_i} \times 100\%$$

Table 3. The annual SO₂ emissions estimated in three inventories at given air quality monitoring sites in downtown Nanjing.

SO ₂ /Mg	National (MEIC)	Regional (Fu et al., 2013)	Provincial (this work)
XWH	1297.5	1790.9	411.0
RJL	1297.5	1720.8	303.1
ZHM	1297.5	1918.3	396.2
CCM	928.6	1635.3	371.8
MGQ	1297.5	478.6	395.0

Table 4. The monthly mean contributions of power, iron & steel and cement plants to the PM_{2.5} concentrations at the air quality monitoring sites in Nanjing in October 2012.

Monitoring site	Contri. of power (%)			Contri. of iron & steel (%)			Contri. of cement (%)		
	Max.	Min.	Ave.	Max.	Min.	Ave.	Max.	Min.	Ave.
XWH/SXL	52	-6	8	82	-2	14	43	-1	8
RJL	42	-6	7	79	0	11	44	0	9
ZHM	44	-5	7	71	-3	12	48	0	9
CCM	32	-8	7	83	-4	13	58	-5	8
MGQ	58	-5	9	89	-2	8	35	-5	7
XLS	35	-5	7	67	-3	10	57	0	10
PKS	65	-6	7	77	-1	11	45	-1	7
OCS	33	-7	7	87	0	12	58	0	8

Note: Max., min., ave. and contri. indicate maximum, minimum, average and contribution, respectively.

Figure 1

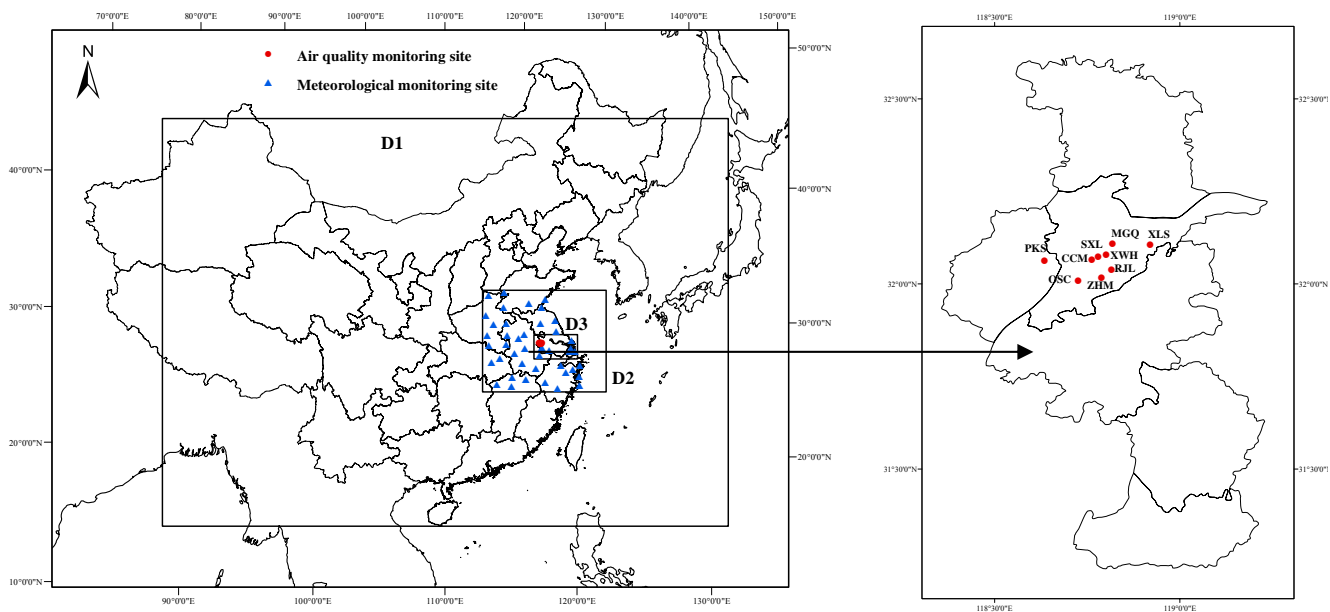


Figure 2

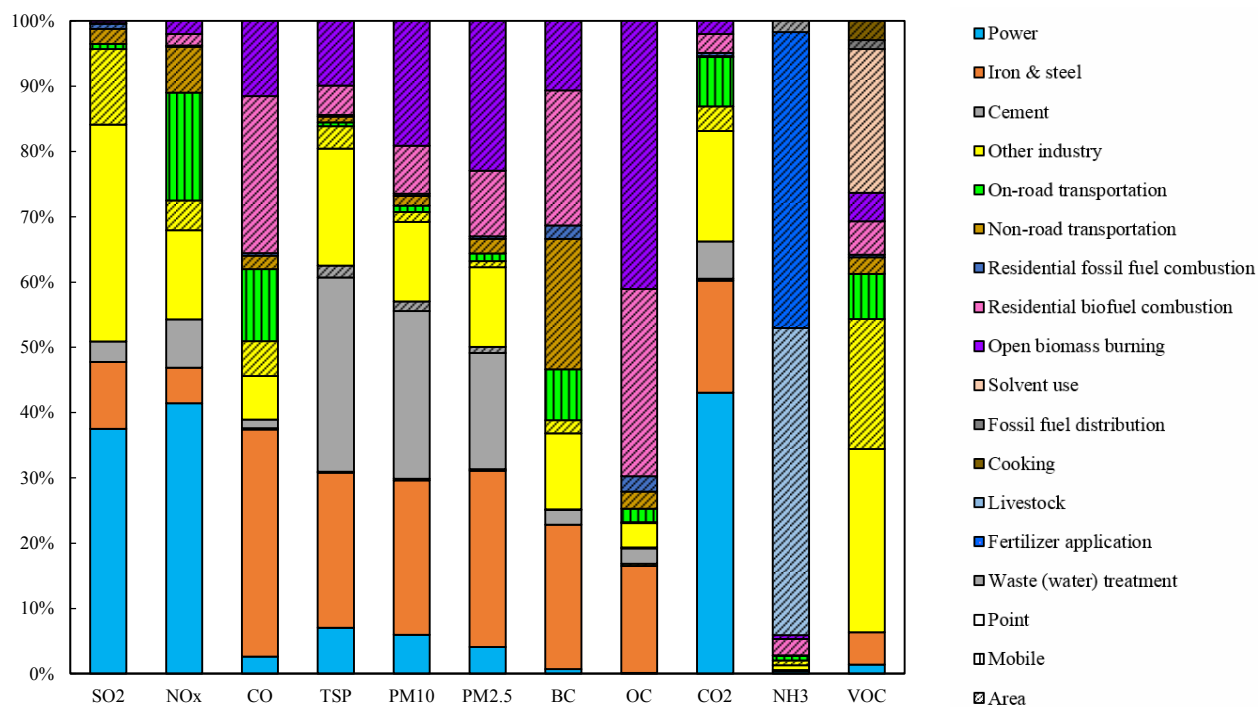


Figure 3

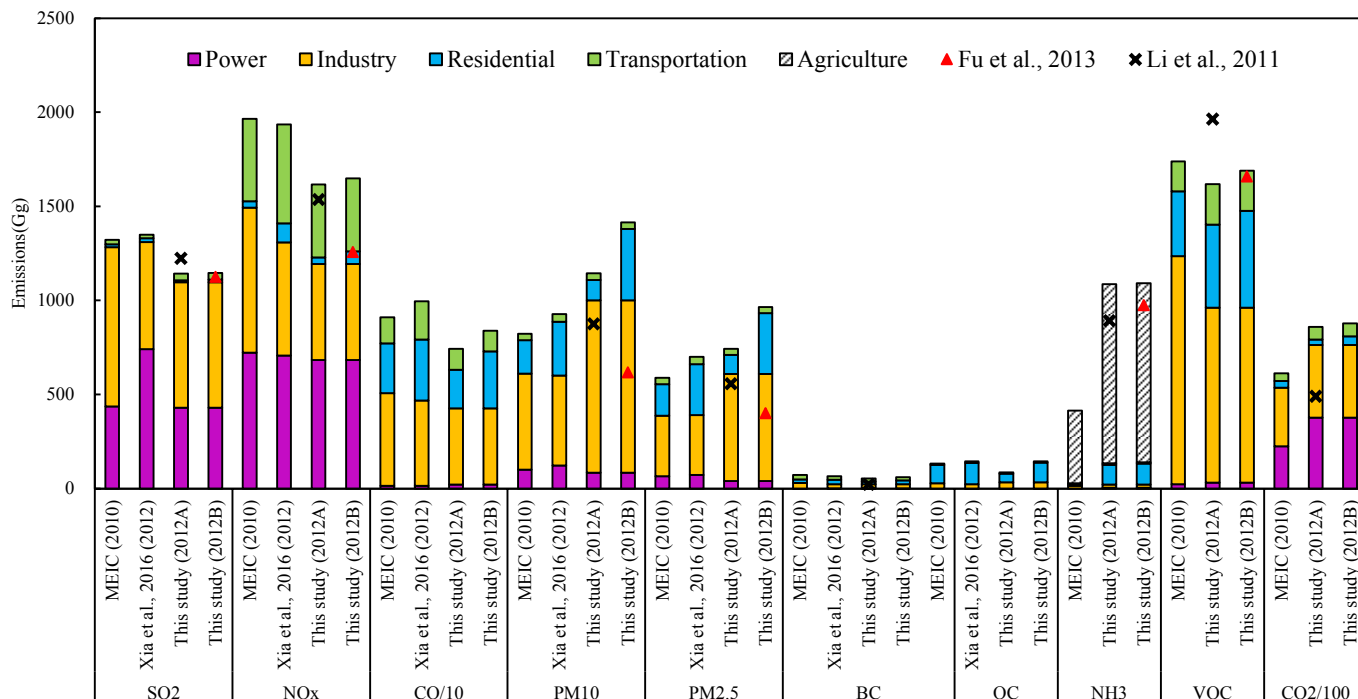


Figure 4

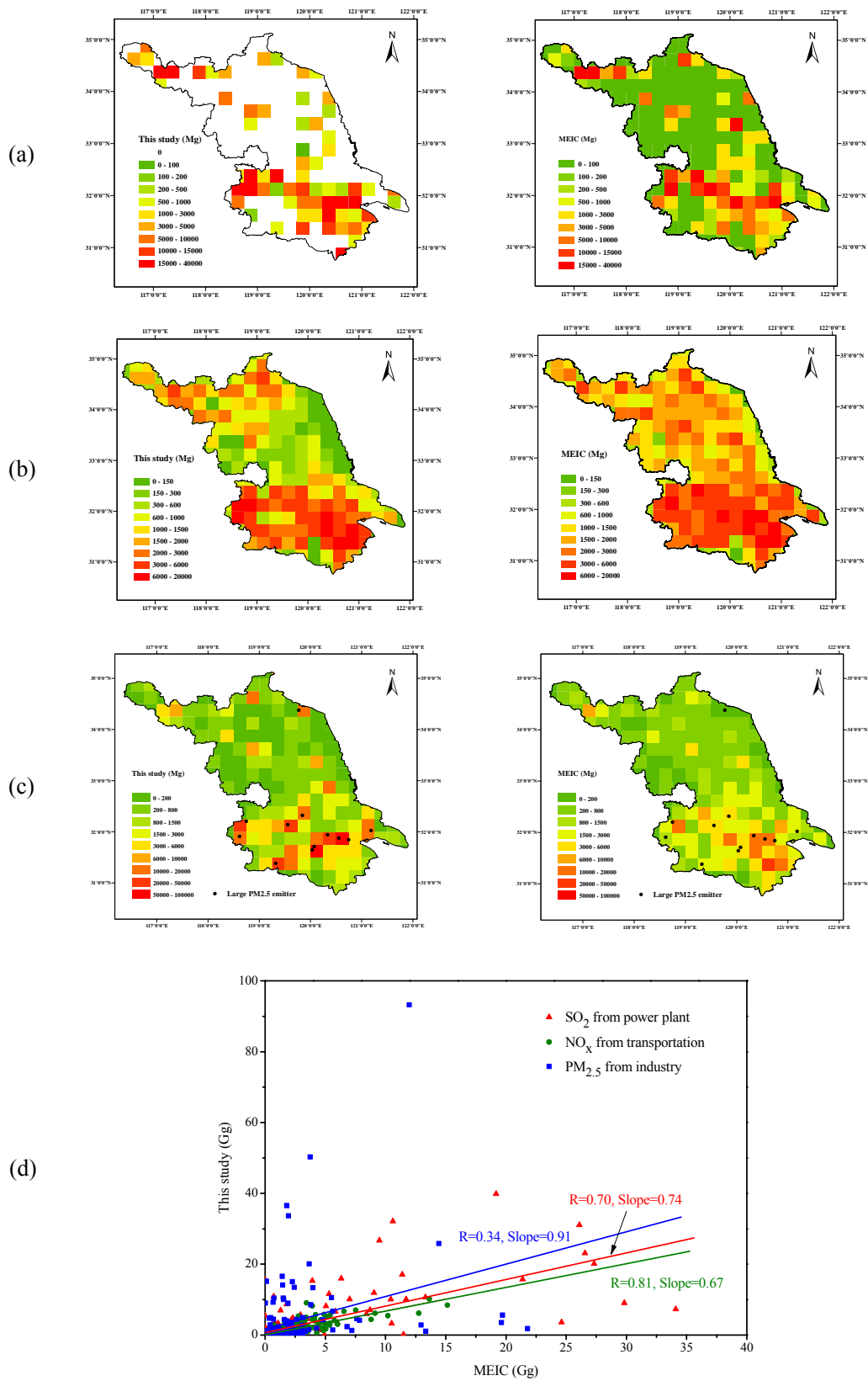


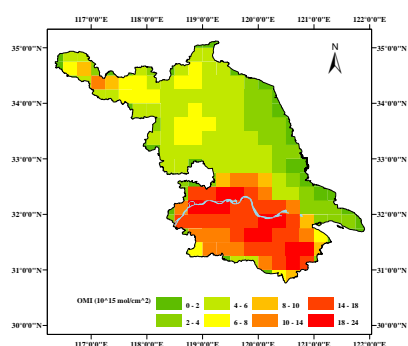
Figure 5

NO₂ VCDs

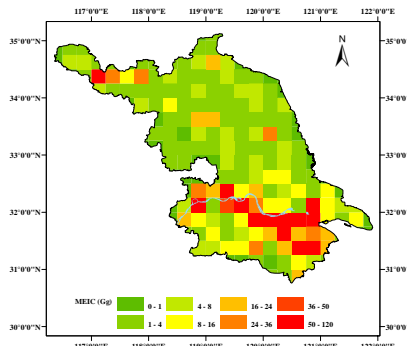
NO_x emission

Linear regression

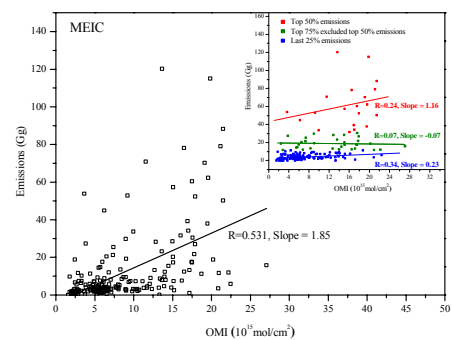
2010



(a)

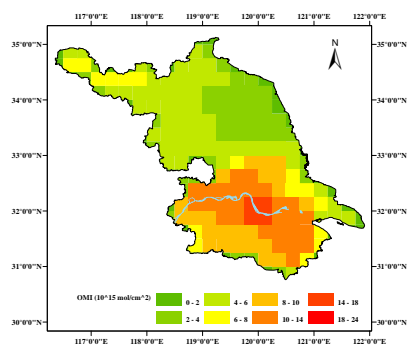


(c)

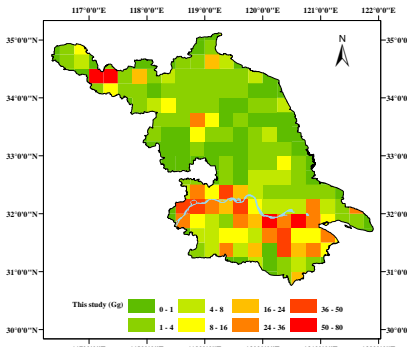


(e)

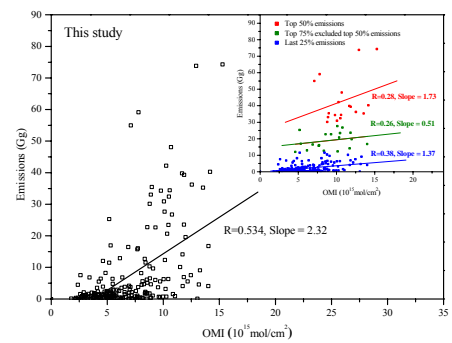
2012



(b)



(d)



(f)

Figure 6

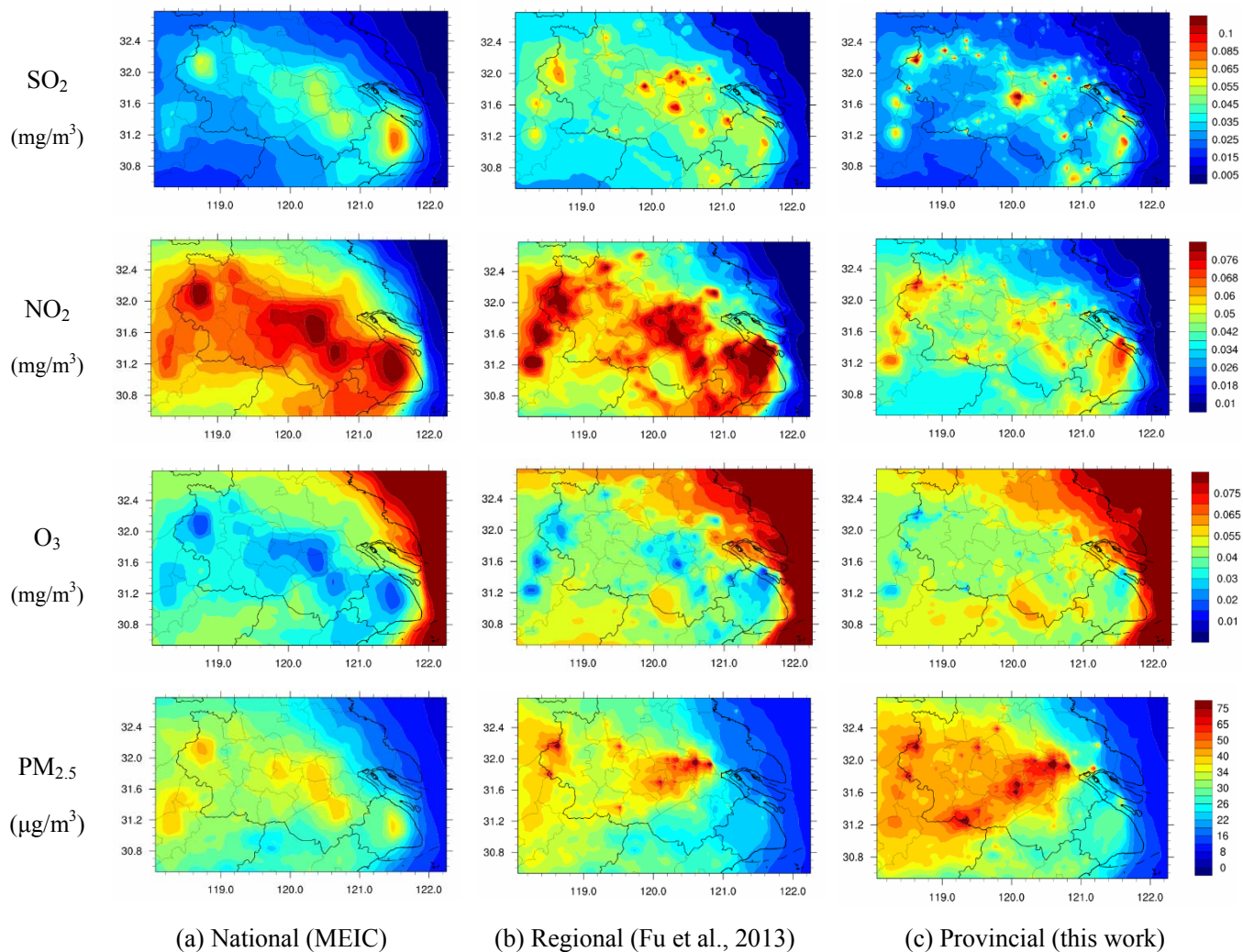
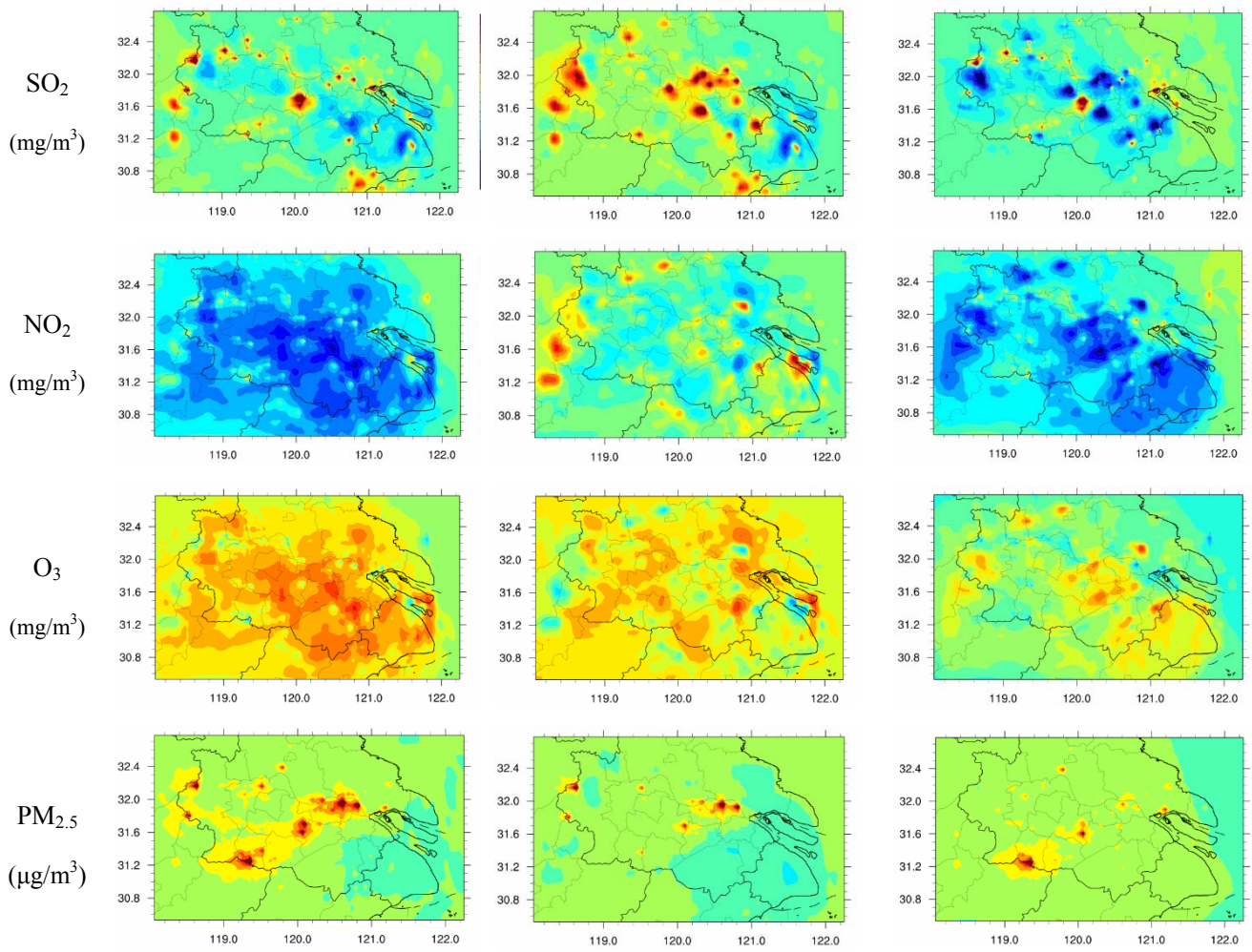


Figure 7



(a) Provincial – national

(b) Regional – national

(c) Provincial – regional

Figure 8

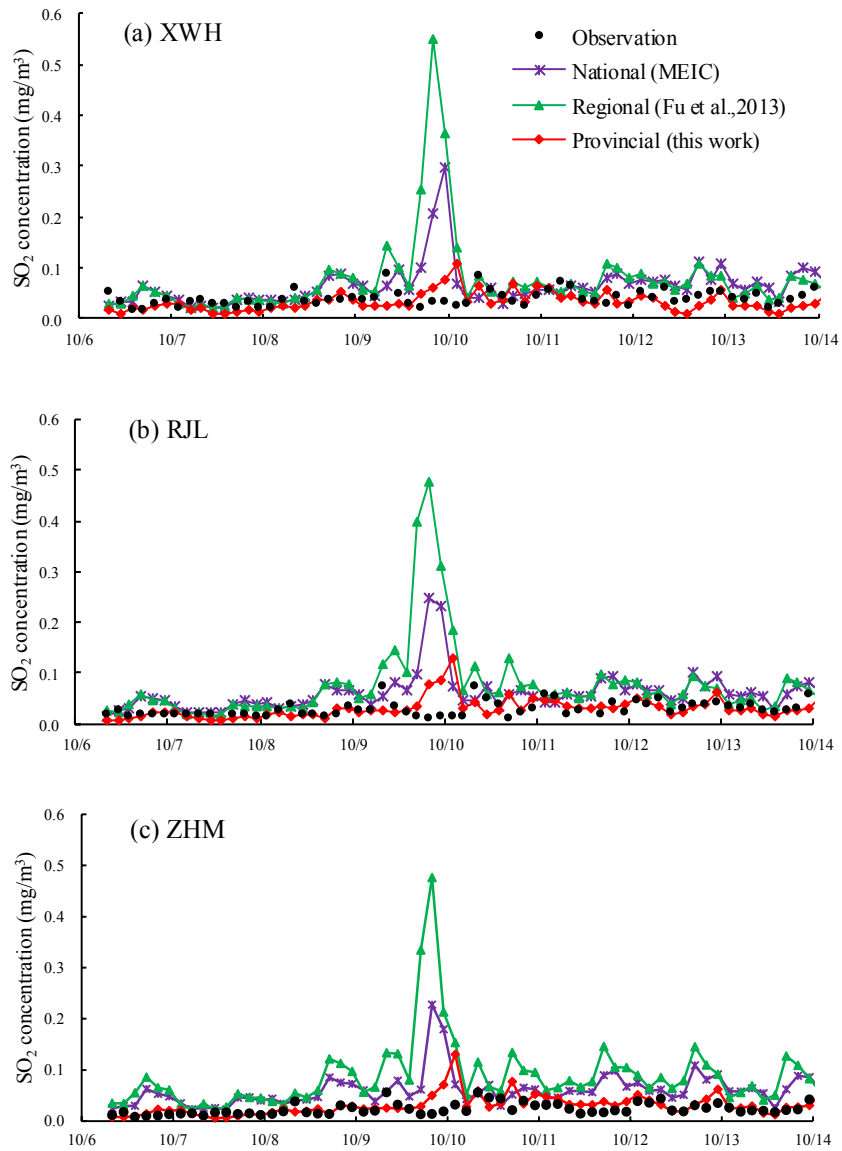
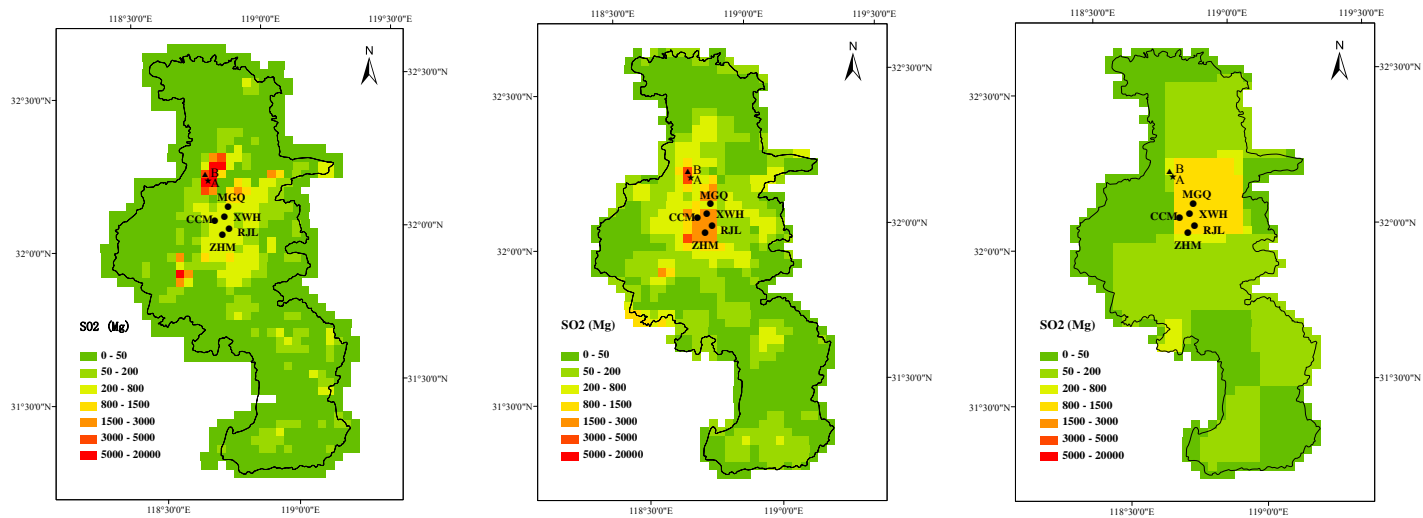


Figure 9

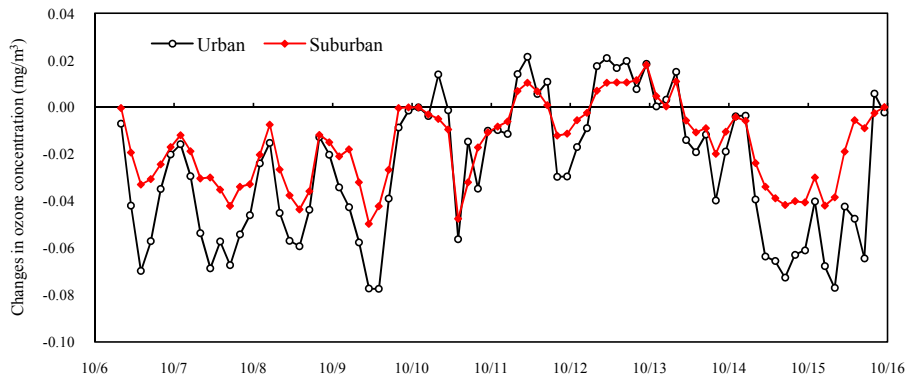


(a)

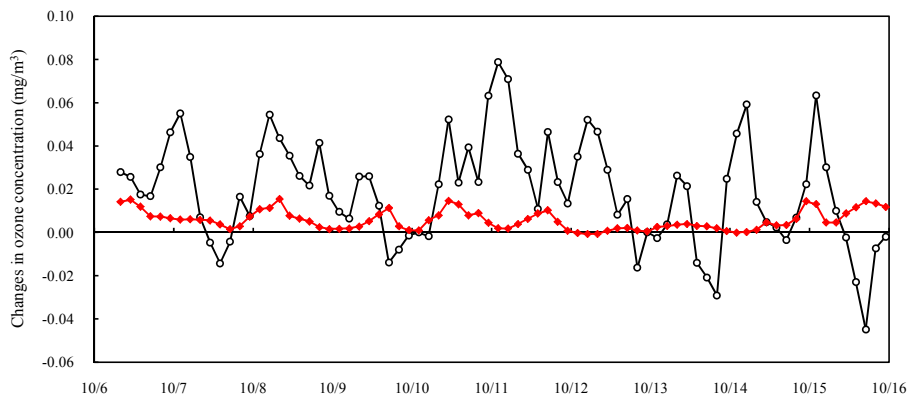
(b)

(c)

Figure 10



(a)



(b)